

1 Development, intercomparison and evaluation of an improved 2 mechanism for the oxidation of dimethyl sulfide in the UKCA model

3 Ben A. Cala^{1,*}, Scott Archer-Nicholls^{1,#}, James Weber^{1,\$}, N. Luke Abraham^{1,2}, Paul T. Griffiths^{1,2}, Lorrie
4 Jacob¹, Y. Matthew Shin¹, Laura E. Revell³, Matthew Woodhouse⁴, Alexander T. Archibald^{1,2}

5 ¹Yusuf Hamied Department of Chemistry, University of Cambridge, Cambridge, CB2 1EW, UK

6 ²National Centre for Atmospheric Science, Cambridge, CB2 1EW, UK.

7 ³School of Physical and Chemical Sciences, University of Canterbury, Christchurch, New Zealand.

8 ⁴CSIRO Oceans and Atmosphere, Aspendale, 3195, Australia.

9 ^{*}Now at Department of Ocean Systems (OCS), NIOZ Royal Netherlands Institute for Sea Research, Texel, the Netherlands

10 [#]Now at IT Services, University of Manchester, Manchester, M13 9PL, UK.

11 ^{\$}Now at School of Biosciences, University of Sheffield, S10 2TN, UK.

12
13 *Correspondence to:* Alexander T. Archibald ata27@cam.ac.uk and Ben. A. Cala ben.cala@nioz.nl
14

15 **Abstract.** Dimethyl sulfide (DMS) is an important trace gas emitted from the ocean. The oxidation of DMS has long been
16 recognised as being important for global climate through the role DMS plays in setting the sulfate aerosol background in the
17 troposphere. However, the mechanisms in which DMS is oxidised are very complex and have proved elusive to accurately
18 determine in spite of decades of research. As a result the representation of DMS oxidation in global chemistry-climate models
19 is often greatly simplified.

20
21 Recent field observations, laboratory and *ab initio* studies have prompted renewed efforts in understanding the DMS oxidation
22 mechanism, with implications for constraining the uncertainty in the oxidation mechanism of DMS as incorporated in global
23 chemistry-climate models. Here we build on recent evidence and develop a new DMS mechanism for inclusion in the UK
24 Chemistry Aerosol (UKCA) chemistry-climate model. We compare our new mechanism (CS2-HPMTF) to a number of
25 existing mechanisms used in UKCA (including the highly simplified 3 reactions, 2 species, mechanism used in CMIP6 studies
26 with the model) and to a range of recently developed mechanisms reported in the literature through a series of global and box
27 model experiments. Global model runs with the new mechanism enable us to simulate the global distribution of hydroperoxyl
28 methyl thioformate (HPMTF), which we calculate to have a burden of 2.6-26 Gg S (in good agreement with the literature
29 range of 0.7-18 Gg S). We show that the sinks of HPMTF dominate uncertainty in the budget, not the rate of the isomerisation
30 reaction forming it, and that based on the observed DMS/HPMTF ratio from the global surveys during the NAS Atmospheric
31 Tomography mission (ATom), rapid cloud uptake of HPMTF worsens the model-observation comparison. Our box model
32 experiments highlight that there is significant variance in simulated secondary oxidation products from DMS across
33 mechanisms used in the literature, with significant divergence in the sensitivity of the rates of formation of these products to

34 temperature exhibited; especially for methane sulfonic acid (MSA). Our global model studies show that our updated DMS
35 scheme performs better than the current scheme used in UKCA when compared against a suite of surface and aircraft
36 observations. However, sensitivity studies underscore the need for further laboratory and observational constraints. In
37 particular our results suggest that as a priority long-term DMS observations be made to better constrain the highly uncertain
38 inputs into the system and laboratory studies be performed that address: 1) the uptake of HPMTF onto aerosol surfaces and
39 the products of this reaction. 2) The kinetics and products of the following reactions: CH_3SO_3 decomposition; $\text{CH}_3\text{S} + \text{O}_2$;
40 CH_3SOO decomposition; $\text{CH}_3\text{SO} + \text{O}_3$.

41

42 **1 Introduction**

43 It is estimated that 16-28 Tg S year⁻¹ are emitted in the form of dimethyl sulfide (DMS, CH_3SCH_3) from the ocean, making
44 DMS the most abundant biological source of sulfur in the Earth system (Andreae, 1990, Tesdal et al., 2015, Bock et al., 2021).
45 Elucidating the atmospheric fate of DMS has been a long standing goal of the atmospheric chemistry research community
46 owing to a proposed biogeochemical feedback cycle (CLAW; Charlson et al. 1987), whereby DMS oxidation is key to a
47 homeostatic feedback loop. The initial steps in DMS oxidation are well understood (Barnes et al., 2006). Focusing on oxidation
48 via OH (NO_3), the most important oxidant during the daytime (nighttime), DMS is oxidised in the gas-phase through two main
49 pathways: the abstraction pathway forms the methylthiomethylperoxy radical (MTMP, $\text{CH}_3\text{SCH}_2\text{OO}$) in the first step, while
50 the addition pathway leads to dimethyl sulfoxide (DMSO, CH_3SOCH_3 ; and to a lesser extent DMSO_2) as an important
51 intermediate.

52 $\text{DMS} + \text{OH}/\text{NO}_3 \rightarrow \text{MTMP} + \text{H}_2\text{O}/\text{HNO}_3$ (abstraction)

53 $\text{DMS} + \text{OH} \rightarrow \text{DMSO} + \text{HO}_2$ (addition)

54 Ultimately, the oxidation of DMS leads to products such as H_2SO_4 and sulfate (SO_4^{2-}), as these represent the highest oxidation
55 states of sulfur (S(VI)). Along the way from DMS, a number of secondary oxidation products such as sulfur dioxide (SO_2),
56 methane sulfonic acid (MSA, $\text{CH}_3\text{SO}_3\text{H}$) and carbonyl sulfide (OCS) can be formed, however the yields of these species
57 depend on the mechanisms involved, which themselves are a function of the chemical (e.g., levels of oxidants) and
58 environmental conditions (e.g., temperature and humidity). The yields of these products are relatively uncertain, with estimates
59 of the DMS-to- SO_2 yield spanning 14-96 % (von Glasow and Crutzen, 2004). The oxidation products can participate in aerosol
60 growth and in new particle formation, affecting the number of cloud condensation nuclei (CCN). As such DMS oxidation can
61 impact cloud formation and lifetime and hence climate; although the absolute effect is still highly uncertain due to the
62 uncertainty in the kinetics and mechanisms of DMS oxidation. Indeed, natural aerosols such as DMS contribute to large
63 uncertainties in the radiative forcing of the pre-industrial atmosphere (Carslaw et al., 2013; Fung et al., 2022).

64

65 Substantial discrepancies between different DMS oxidation mechanisms under different conditions have been found (de Bryn
66 et al., 2002; von Glasow and Crutzen, 2004). The intercomparison study by Karl et al. (2007) looked at seven different
67 chemistry schemes in a box model (using the same inputs) and observed that SO₂ mixing ratios varied from 2 to 44 ppt.
68 Differences between models are even greater when looking at MSA yield (Karl et al., 2007, Hoffmann et al., 2021). The large
69 uncertainties of product ratios indicate the need for more observational constraints for DMS chemistry in models.

70 In the UK Chemistry and Aerosol model (UKCA) two different chemistry schemes are implemented: StratTrop (Archibald et
71 al., 2020), which is a simplified chemistry mechanism included in the UK Earth System Model (Sellar et al., 2019) and CRI-
72 Strat2 (Archer Nicholls et al., 2021; Weber et al., 2021). The DMS oxidation mechanism in StratTrop is, like those used in
73 many Earth System Models (ESMs), a very simple scheme (see S1.4.1 for more details). We believe modellers have opted to
74 keep the DMS chemistry incredibly simple for two main reasons 1) numerical efficiency 2) uncertainty in what to do owing
75 to lack of detailed DMS oxidation mechanisms that have been calibrated against laboratory data. The StratTrop DMS
76 mechanism only includes four reactions and no intermediates for the DMS oxidation scheme.



81 Omitting intermediates might lead to a misrepresentation of the spatial distribution of oxidation products and an overestimation
82 in their formation since the intermediates might be subject to wet and dry deposition or cloud uptake. Because a unity yield of
83 SO₂ is assumed, a change in the distribution of oxidation products due to a changing climate cannot be evaluated.

84
85 CRI-Strat2 (hereafter CS2) (Archer-Nicholls et al., 2021, Weber et al., 2021) is a mechanism that aims to be of intermediate
86 complexity. CS2 includes 19 reactions and 7 intermediates (DMSO, MSIA, MTMP, CH₃S, CH₃SO, CH₃SO₂, CH₃SO₃) as part
87 of its DMS scheme and is primarily based on the work of von Glasow and Crutzen (2004). Whilst the CS2 DMS mechanism
88 is much more complex than the StratTrop scheme, it represents an understanding of DMS chemistry that is far from up-to-
89 date.

90
91 In this work, the gas-phase DMS oxidation by OH and NO₃ in CS2 is updated according to the current scientific understanding.
92 The greatest update is the inclusion of the recently discovered intermediate hydroperoxymethyl thioformate (HPMTF,
93 HOOCH₂SCHO), which is formed through the autoxidation of the methylthiomethyl peroxy radical (MTMP, CH₃SCH₂OO)
94 in the abstraction pathway (Wu et al., 2015, Berndt et al., 2019, Veres et al. 2020). Currently, it is estimated that ~30-50% of
95 DMS yields HPMTF (Veres et al., 2020; Novak et al. (2021); Fung et al. (2022)). There are large uncertainties about the value
96 of $k_{\text{isom},1}$, the rate constant of the first H-shift, which is the rate determining step for HPMTF formation (**Figure 1**). (Note, given
97 that the first isomerization step is rate limiting, the overall rate constant for isomerization is denoted k_{isom}). This determines if

98 autoxidation can compete with or surpass the bimolecular reactions of MTMP with HO₂ and NO. The chamber study by Ye et
99 al. (2021) estimates a probability distribution based on their measurements with one geometric standard deviation spanning an
00 order of magnitude. The isomerization rate constant is predicted using *ab initio* methods to be strongly temperature dependent,
01 indicating that this pathway could be more relevant under a warming climate (Wu et al., 2015; Veres et al., 2020). Following
02 the closure of the Discussion version of this manuscript the first temperature-dependent direct kinetic study of the isomerization
03 of rate constant for MTMP to HPMTF was published (Assaf et al., 2023). In that study the authors calculate the Arrhenius
04 temperature barrier as 7278 ± 99 K, confirming the high temperature dependence of the reaction experimentally.

05
06 As of now, the fate of HPMTF in the atmosphere is largely unknown. Wu et al. (2015) postulate further oxidation with OH,
07 ultimately yielding SO₂ as the dominant product and OCS as a side product. Veres et al. (2020) observe an abrupt decrease of
08 HPMTF mixing ratio in clouds and therefore suggest that heterogeneous loss to aerosol and cloud uptake plays a big role.
09 Vermeuel et al. (2020) support this hypothesis: they find a diurnal profile of HPMTF in the vicinity of California's coast and
10 suggest this is due to the consistent diurnal profile of cloud present. This hypothesis is further supported by the study by Novak
11 et al. (2021), which looks at two case studies and concludes that cloud uptake determines the lifetime of HPMTF. Novak et
12 al. (2021) found that cloud-uptake of HPMTF reduces SO₂ production from DMS by over a third, while providing a more
13 direct pathway to sulfate formation. On the contrary, the chamber study and calculation of Henry's law constant by Wollesen
14 de Jonge et al. (2021) predict that HPMTF does not directly contribute to new particle formation or aerosol growth. Instead,
15 their study proposes aqueous oxidation by OH, ultimately still yielding gas-phase SO₂. Khan et al. (2021) stress the importance
16 of photolysis as a potential loss pathway, which might explain the observed diurnal concentrations throughout the day. Overall,
17 loss processes of HPMTF are poorly understood.

18
19 In this work, we perform a series of updates to the CS₂ DMS oxidation scheme which are evaluated against the current CS₂
20 and the very simplified DMS chemistry in StratTrop. The aim of this work is to improve the representation of DMS chemistry
21 in UKCA and determine the influence of some of the major mechanistic uncertainties on model simulated SO₂ levels compared
22 against ATom observations (Wofsy et al., 2018; Veres et al., 2020). Our study includes a comprehensive set of box model
23 studies, including an intercomparison of our new DMS scheme against other recently reported schemes in the literature, and
24 global 3D simulations with the UKCA model. To complement the work of Fung et al. (2022), sensitivity studies with variable
25 rates of production, and cloud and aerosol uptake of HPMTF are performed to investigate the effects of the uncertainty in
26 HPMTF formation and depletion on the distribution and burden of SO₂ and sulfate (given their importance in climate) using
27 a structurally different model to that they used.

28

29 **2 Methods**

30 **2.1 Model description**

31 **2.1.1 Set up**

32 **Box model**

33 For the box model experiments, BOXMOX (Knote et al., 2015), the box modelling extension to the Kinetic PreProcessor
34 (KPP) (Sandu and Sander, 2006) was used. The initial and background concentrations of the species were set to be
35 representative of the remote marine boundary layer (MBL) (and are detailed in **Table S1**). NO_x concentration was kept at
36 approximately 10 ppt, unless otherwise specified.

37 The box model set up simulates an MBL air parcel exchanging with the free troposphere. The diurnal profile of the planetary
38 boundary layer height was modelled after the diurnal profile of the MBL in Ho et al. (2015) (**Table S2**). Mixing of the air
39 within the box with the free troposphere is described by the increases of box height: it is assumed that changes in the box
40 volume are due to the influx of background air. Emissions of DMS are added at 3.48×10^9 molec. cm⁻² s⁻¹ (consistent with
41 the higher emission flux in von Glasow and Crutzen (2004)). Emissions mix instantaneously within the box. Temperature
42 varies throughout a 24-hour period between 289-297 K, with a mean of 293 K (**Table S2**). Photolysis reactions are scaled
43 depending on the time of day, and make use of the pre-calculated “J” rates obtained from the MCMv3.3.1. The simulations
44 were run for 192 hours (8 days) with 10-minute time steps. CRI v2.2 R5 (CS2) (Jenkin et al., 2019; Weber et al., 2021) was
45 employed as the base chemical mechanism. Unless otherwise specified, only reactions of the DMS scheme were changed.
46 Neither dry nor wet deposition was included in the box model experiments. The analysis of the BOXMOX simulations
47 discussed in Section 3.1.1 and 3.2.1 focuses on the continuous (hourly) output. In Section 3.1.2 and 3.2.2, simulations with a
48 prescribed temperature (260 - 310 K, step size: 5 K) were conducted. The data from day 7 and 8 of the runs was averaged to
49 enable the effects of changes in the temperature on species concentration simulated in the box model to be calculated (following
50 Archibald et al., 2010)

51

52 **3D simulations**

53 For the 3D simulations we use UKCA, the chemistry and aerosol component of UKESM1, with a horizontal resolution of
54 $1.25^\circ \times 1.875^\circ$ with 85 vertical levels up to 85 km (Walters et al., 2019). UKCA uses the GLOMAP-mode aerosol scheme,
55 which simulates sulfate, sea salt, black carbon (BC), organic matter, and dust but does not currently simulate nitrate aerosol
56 (Mulcahy et al., 2020). Simulations were run for 18 months, using the first 6 months as spin up. In order to look at high time
57 resolution output simulations were re-run for limited time periods using the re-start files of the longer runs but outputting data
58 at hourly frequency.

59

60 Temperature and horizontal wind fields were nudged (Telford et al., 2013) in all model runs to the Era-Interim atmospheric
61 reanalysis from ECMWF (Dee et al., 2011). See the SI for further details.

62

63 The emissions used in this study for UKCA are the same as those from Archer-Nicholls et al (2021) and are those developed
 64 for the Coupled-Model Intercomparison Project 6 (CMIP6) (Collins et al., 2017). See the SI for further details. Oceanic
 65 emissions of DMS are calculated from seawater DMS concentrations (Sellar et al., 2019). In the atmosphere-only setup
 66 employed here seawater DMS concentrations for 2014 from a UKESM1 fully-coupled SSP3-70 ensemble member were
 67 prescribed. The DMS emission flux from the ocean used in the model was 16 Tg S yr⁻¹ and therefore on the low end of estimates
 68 of oceanic DMS emissions (e.g., Lana et al., 2011; Bock et al., 2021).

69

70

71 2.1.2 Model runs

72

73 **Table 1:** Configuration of model runs in this study. The last two columns indicate whether this scheme was used for the
 74 BOXMOX experiments or the UKCA runs or both. Additional BOXMOX simulations were performed and the results of which
 75 are included in the Supplementary Information (SI) for completeness.

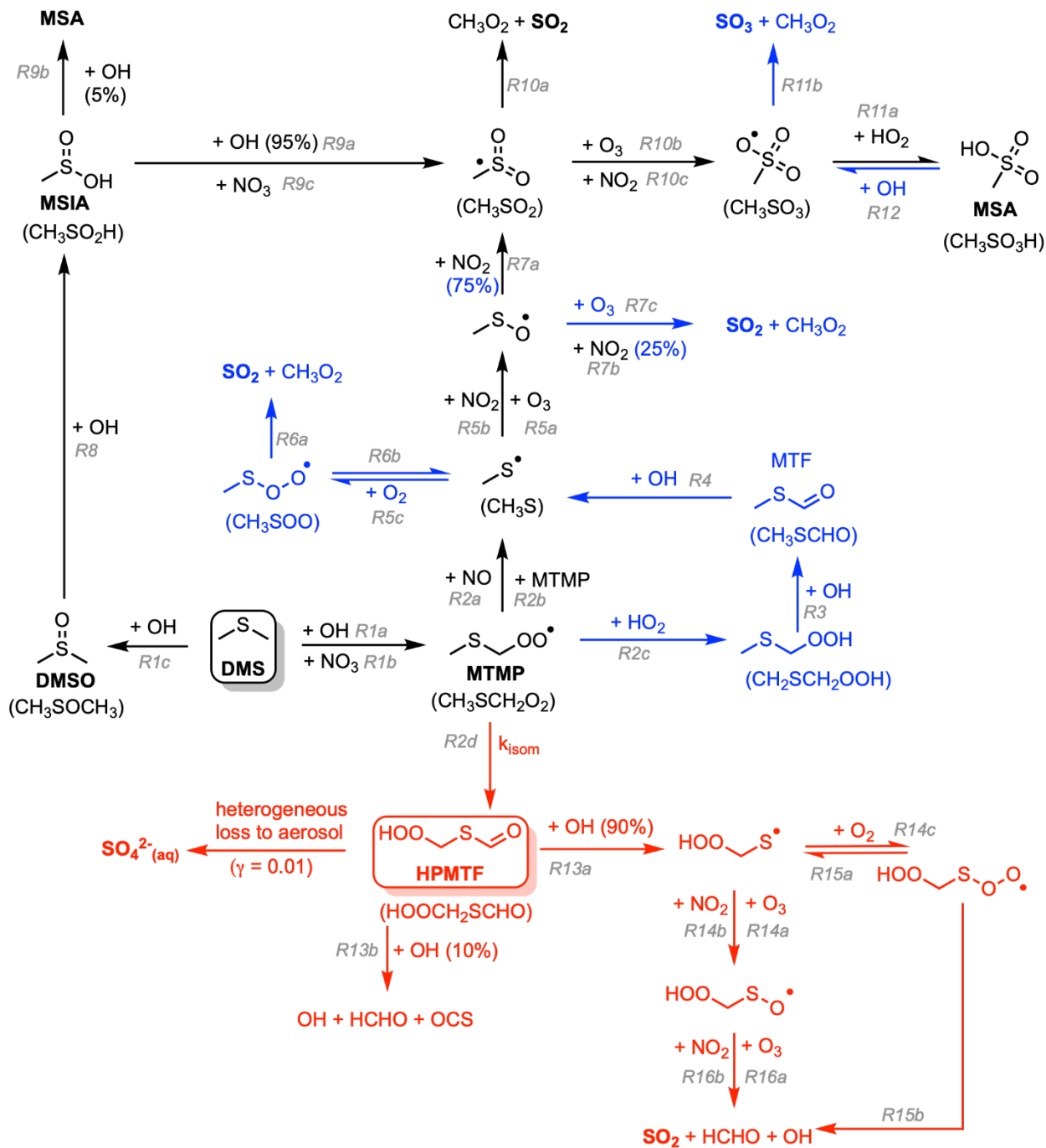
Alias	Description	Used for:	
		BOXMOX	UKCA
CS2	Base simulation, standard CRIStrat2 (or CRIV2.2R5) scheme	✓	✓
ST	StratTrop chemistry scheme ($ST - CS2 = \Delta ST$; change between ST and CS2)	✓	✓
ST~CS2	StratTrop DMS scheme but CS2 oxidants ($ST\sim CS2 - CS2 = \Delta CC$; change between CS2 and the ST DMS scheme only)	✓	-
CS2-HPMTF	CS2 + updates in Table 2 and Table 3 ($CS2\text{-HPMTF} - CS2 = \Delta UPD$; effects of all updates made to the scheme)	✓	✓
CS2-UPD-DMS	CS2 + updates in Table 2 = CS2-HPMTF - updates in Table 3 ($CS2\text{-HPMTF} - CS2\text{-UPD-DMS} = \Delta HPMTF$; effects of the isom. pathway only)	✓	-
CS2-HPMTF-CLD	CS2-HPMTF + cloud and aerosol uptake ($\gamma = 0.01$) ($CS2\text{-HPMTF-CLD} - CS2\text{-HPMTF} = \Delta CLD$; gives the effects of cloud and aerosol uptake of HPMTF)	-	✓
CS2-HPMTF-FL	CS2-HPMTF + faster total loss of HPMTF to OH ($5.5 \times 10^{-11} \text{ s}^{-1}$) ($CS2\text{-HPMTF-FL} - CS2\text{-HPMTF} = \Delta FL$; gives the effects of faster gas phase loss of HPMTF)	SI	✓
CS2-HPMTF-FP	CS2-HPMTF + isomerisation A-factor scaled by a factor of 5, see Wollesen de Jonge et al. (2021)) ($CS2\text{-HPMTF-FP} - CS2\text{-HPMTF} = \Delta FP$; gives the effects of faster HPMTF production)	SI	✓

76

77 Simulations are performed with the standard or updated DMS scheme to quantify the impacts of the mechanistic changes.
78 Details are given in **Table 1**. We chose as our base run a simulation with the CRIStrat2 chemistry scheme hereafter referred
79 to as CS2 (Weber et al., 2021). We perform two simulations with StratTrop (hereafter ST): ST is the default mechanism as
80 used in UKESM1, while ST~CS2 uses the ST DMS chemistry (R1-R4) but all other reactions (HO_x, NO_x, VOC etc) are
81 identical to CS2. This allows us to attribute the changes arising solely to differences in the oxidising capacity/environment
82 (driven by the chemistry not strongly coupled to DMS) and isolate the role due to differences in the DMS reactions themselves.
83

84 In updating the representation of DMS chemistry for UKCA a number of changes were considered. Broadly these fall into two
85 categories: 1) Incorporation of the chemistry of HPMTF (shown in red in **Figure 1**) 2) updates to other aspects of DMS
86 oxidation chemistry (shown in blue in **Figure 1**). CS2-HPMTF is used to identify the fully updated DMS mechanism (**Table**
87 **2, Table 3**). All other runs act as sensitivity runs. CS2-UPD-DMS allows the evaluation of only updating the standard DMS
88 chemistry (**Table 2**), without the addition of the isomerization branch and HPMTF formation (**Table 3**). CS2-HPMTF-CLD
89 adds cloud and aerosol uptake of HPMTF with subsequent sulfate formation, similar to Novak et al. (2021). With CS2-
90 HPMTF-FP and CS2-HPMTF-FL the effects of faster production and faster loss of HPMTF can be assessed.

91
92



93

94 **Figure 1.** Schematic summary of the changes and additions to the gas-phase DMS oxidation mechanism in CS₂. The current
 95 chemistry in CS₂ (Weber et al., 2021) is in black, changes associated with CS₂-UPD-DMS are shown in blue and changes
 96 associated with the addition of the isomerization pathway for CS₂-HPMTF in red.

97

98 2.2 New mechanism development

99 The current CS₂ DMS oxidation mechanism is based on von Glasow and Crutzen (2004). This mechanism is based on an
 100 outdated understanding of DMS oxidation, which excludes key pathways and intermediates that are now known to be well
 101 established (Barnes et al., 2006) as well as more recent pathways and products that have been shown to be important (Veres
 102 et al., 2020). Our aim with the development of the new mechanism is to build upon the existing mechanism in CS₂ and to
 103 update and extend it. To this end we performed a literature review and constructed a number of mechanistic variants that were
 104 examined in a series of box model experiments (see the SI for further details). As with all mechanism development exercises,
 105 a series of target compounds were chosen to reduce the mechanism to achieve a scheme that is parsimonious; for use in a 3D
 106 chemistry-climate model. In our study we chose DMS, SO₂, sulfate (H₂SO₄) and HPMTF as the key target molecules for
 107 mechanism optimization. **Figure 1** shows the two-step improvement of this mechanism. First, the improvement of the standard
 108 chemistry by updating rate constants for existing reactions in the scheme or the addition of reactions that were missing (denoted
 109 with blue colouring in **Figure 1**), and second, the addition of the HPMTF pathway (in red in **Figure 1**). The focus in this study
 110 is on gas-phase DMS oxidation by OH and NO₃. Our prime focus is on the primary oxidation products (DMSO and MTMP)
 111 and their subsequent chemistry. While other studies include DMS oxidation by BrO and Cl, the contribution is either negligible
 112 or there is a large uncertainty attached due to substantial discrepancies between/within models and measurements of halogens
 113 and halogen oxides (Wang et al., 2021; Fung et al., 2022). Moreover, UKCA doesn't currently have a comprehensive
 114 tropospheric halogen mechanism and levels of BrO and Cl simulated are much lower than observations suggest.

15
 16 The updates made to the standard CRIStrat 2 DMS scheme are presented in Tables 2 and 3. Please see the SI S1.2 for a
 17 complete description of how these updates were made.

18
 19
 20 **Table 2:** Summary of the H-abstraction and OH-addition branches in the DMS oxidation pathway. Reactions in **bold** are
 21 newly added in this work.

No.	Reactions	Rate (cm ³ molecule ⁻¹ s ⁻¹)	Reference
1a	DMS + OH → MTMP + H ₂ O	$1.12 \times 10^{-11} \exp^{(-250/T)}$	IUPAC SOx22 (upd. 2006)
1b	DMS + NO ₃ → MTMP + HNO ₃	$1.90 \times 10^{-13} \exp^{(520/T)}$	Atkinson et al. (2004)
1c	DMS + OH → DMSO + HO ₂	see note ^a	IUPAC SOx22 (upd. 2006)
2a	MTMP + NO → HCHO + CH ₃ S + NO ₂	$4.90 \times 10^{-12} \exp^{(263/T)}$	von Glasow and Crutzen (2004)
2b	MTMP + MTMP → 2 HCHO + 2 CH ₃ S	1.0×10^{-11}	von Glasow and Crutzen (2004)
2c	MTMP + HO₂ → CH₂SCH₂OOH	$2.91 \times 10^{-13} \exp^{(1300/T)} \times 0.387$	MCMv3.3.1
3	CH₂SCH₂OOH + OH → CH₃SCHO	7.03×10^{-11}	MCMv3.3.1
4	CH₃SCHO + OH → CH₃S + CO	1.11×10^{-11}	MCMv3.3.1
5a	CH ₃ S + O ₃ → CH ₃ SO	$1.15 \times 10^{-12} \exp^{(432/T)}$	Atkinson et al. (2004)
5b	CH ₃ S + NO ₂ → CH ₃ SO + NO	$3.00 \times 10^{-12} \exp^{(210/T)}$	Atkinson et al. (2004)

5c	CH₃S + O₂ → CH₃SOO	1.20×10⁻¹⁶ exp^(1580/T) × [O₂]	Atkinson et al. (2004)
6a	CH₃SOO → CH₃O₂ + SO₂	5.60×10⁺¹⁶ exp^(-10870/T)	Atkinson et al. (2004)
6b	CH₃SOO → CH₃S + O₂	3.50×10⁺¹⁰ exp^(-3560/T)	MCMv3.3.1 (based on: McKee (1993), and Butkovskaya and Barnes (2002))
7a	CH ₃ SO + NO ₂ → CH ₃ SO ₂ + NO	1.2×10 ⁻¹¹ × 0.75	Borrisenko et al. (2003), Atkinson et al. (2004)
7b	CH ₃ SO + NO ₂ → SO ₂ + CH ₃ O ₂ + NO	1.2×10 ⁻¹¹ × 0.25	Borrisenko et al. (2003), Atkinson et al. (2004)
7c_old	CH ₃ SO + O ₃ → CH ₃ SO ₂	6.0×10 ⁻¹³	Von Glasow and Crutzen (2004)
7c	CH₃SO + O₃ → CH₃O₂ + SO₂	4×10⁻¹³	Borrisenko et al. (2003), IUPAC SOx61 (upd. 2006)
8	DMSO + OH → MSIA + CH ₃ O ₂	8.7×10 ⁻¹¹ × 0.95	von Glasow and Crutzen (2004)
9a	MSIA + OH → CH ₃ SO ₂ + H ₂ O	9.0×10 ⁻¹¹ × 0.95	von Glasow and Crutzen (2004)
9b	MSIA + OH → MSA + HO ₂ + H ₂ O	9.0×10 ⁻¹¹ × 0.05	von Glasow and Crutzen (2004)
9c	MSIA + NO ₃ → CH ₃ SO ₂ + HNO ₃	1.0×10 ⁻¹³	von Glasow and Crutzen (2004)
10a	CH ₃ SO ₂ → CH ₃ O ₂ + SO ₂	5.0×10 ⁻¹³ exp ^(-9673/T)	MCMv3.3.1 (based on: Barone et al. (1995))
10b	CH ₃ SO ₂ + O ₃ → CH ₃ SO ₃	3.0×10 ⁻¹³	von Glasow and Crutzen (2004)
10c	CH ₃ SO ₂ + NO ₂ → CH ₃ SO ₃ + NO	2.2×10 ⁻¹²	Atkinson et al. (2004)
11a	CH ₃ SO ₃ + HO ₂ → MSA	5.0×10 ⁻¹¹	von Glasow and Crutzen (2004)
11b_old	CH ₃ SO ₃ → CH ₃ O ₂ + H ₂ SO ₄	1.36×10 ¹⁴ exp ^(-11071/T)	von Glasow and Crutzen (2004)
11b	CH₃SO₃ → CH₃O₂ + SO₃	5.0×10¹³ exp^(-9946/T)	MCMv3.3.1 (based on: Barone et al. (1995))
12	MSA + OH → CH₃SO₃	2.24×10⁻¹⁴	MCMv3.3.1

$$^a 9.5 \times 10^{-39} \exp^{(5270/T)} \times [\text{O}_2] / (1 + 7.5 \times 10^{-29} \exp^{(5610/T)} \times [\text{O}_2])$$

23

24 **Table 3:** Summary of the isomerization branch of the H-abstraction pathway. Rate constants referenced to this work are
 25 described in Section S1.2.1 of the SI.

No.	Reaction	Rate (cm ³ molecule ⁻¹ s ⁻¹)	Reference
2d	MTMP → HPMTF + OH	see note ^a	Veres et al. (2020)
13a	HPMTF + OH → HOOCH ₂ S + H ₂ O + CO	1.0×10 ⁻¹¹ × 0.9	this work
13b	HPMTF + OH → OCS + OH + HCHO + H ₂ O	1.0×10 ⁻¹¹ × 0.1	this work
14a	HOOCH ₂ S + O ₃ → HOOCH ₂ SO	1.15×10 ⁻¹² exp ^(430/T)	Wu et al. (2015)
14b	HOOCH ₂ S + NO ₂ → HOOCH ₂ SO + NO	6.00×10 ⁻¹¹ exp ^(240/T)	Wu et al. (2015)
14c	HOOCH ₂ S + O ₂ → HOOCH ₂ SOO	1.20×10 ⁻¹⁶ exp ^(1580/T) × [O ₂]	this work
15a	HOOCH ₂ SOO → HOOCH ₂ S + O ₂	3.50×10 ⁺¹⁰ exp ^(-3560/T)	this work
15b	HOOCH ₂ SOO → HCHO + OH + SO ₂	5.60×10 ⁻¹⁶ exp ^(-10870/T)	this work
16a	HOOCH ₂ SO + O ₃ → HCHO + OH + SO ₂	4×10 ⁻¹³	Wu et al. (2015)
16b	HOOCH ₂ SO + NO ₂ → HCHO + OH + NO + SO ₂	1.2×10 ⁻¹¹	Wu et al. (2015)

26 $a 2.24 \times 10^{+11} \exp(-9800/T) \exp(1.03e8/(T \times T \times T))$

27

28 **2.3 Description of observational data**

29 **2.3.1 The NASA Atmospheric Tomography (ATom) mission**

30 An observational dataset used to compare with the model simulations stems from the fourth flight campaign of the NASA
31 Atmospheric Tomography mission (ATom-4). ATom-4 took place during April and May 2018, and completed a global circuit
32 around the Americas: from the Arctic to the Antarctic over the remote Pacific and Atlantic Ocean at varying altitudes up to 12
33 km. A vast number of atmospheric species were measured, including DMS, HPMTF, and SO₂ (Wofsy et al., 2018).

34

35 In order to compare the 3D model outputs with the data from the ATom-4 campaign, the hourly outputs from the respective
36 model runs were interpolated in regards to time and space to generate the data along the flight path. Only model data at times
37 where valid atmospheric measurements were available are taken into account, resulting in 313 data points for DMS (Whole
38 Air Sampling) and 36,652 for SO₂ (Laser Induced Fluorescence).

39

40 **2.3.2 Surface observations**

41 Other observational measurements are monthly averages (mean) from the years 1990 to 1999 for DMS measurements made
42 on Amsterdam Island (37°S, 77°E) in the southern Indian Ocean (Sciare et al., 2000) and the monthly means from 1991 to
43 1995 for sulfate at the Dumont d'Urville station (66°S, 140°E) at the coast of Antarctica (Minikin et al., 1998). The diel profile
44 of HPMTF as measured at Scripps Pier in July 2018 was taken from Vermeuel et al. (2020). See the SI for the analysis of the
45 modelled and observed DMS mixing ratios.

46 **3 Comparison of DMS oxidation pathways (BOXMOX)**

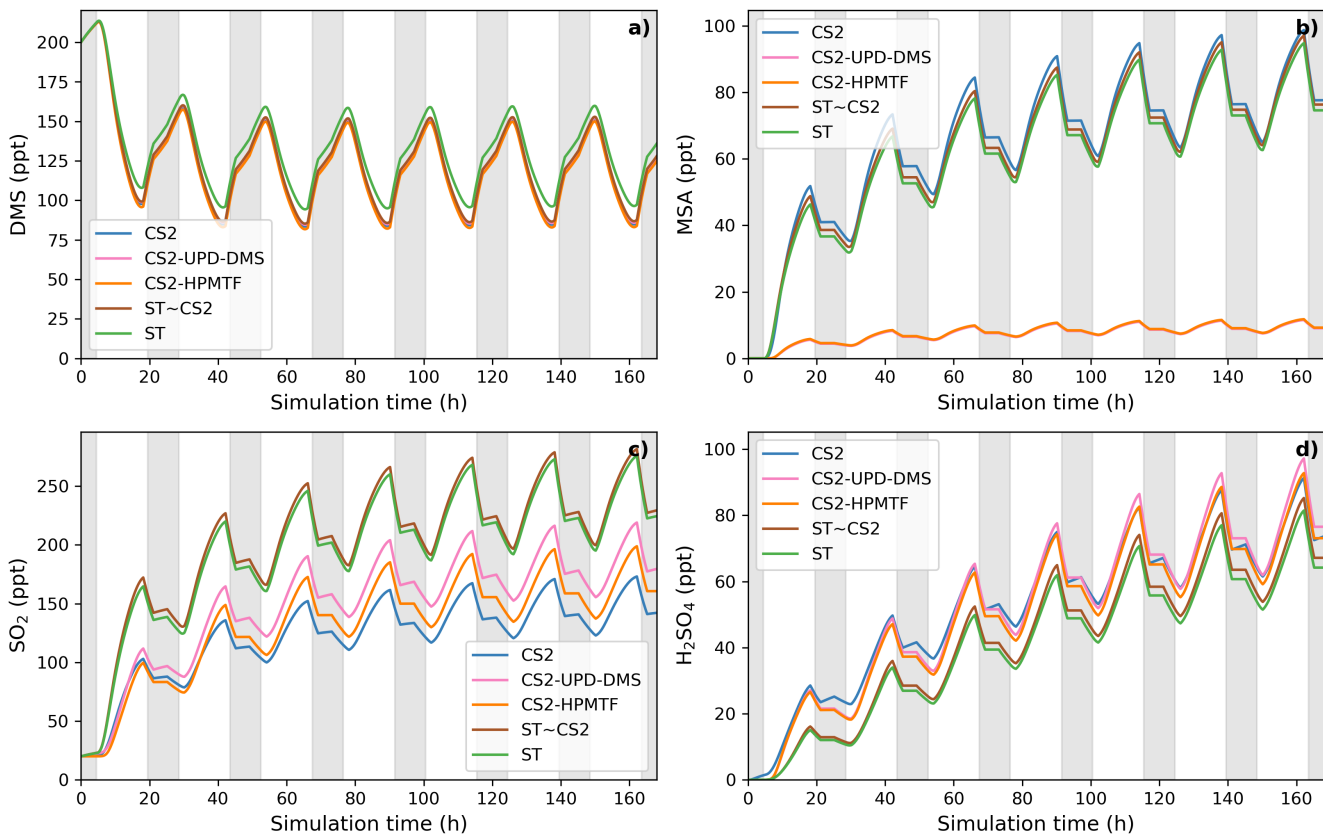
47 Here we present the results of a series of box model simulations using the BOXMOX model (Weber et al., 2020). With
48 BOXMOX we look at the diversity in results from simulations using a range of mechanisms, including our newly developed
49 mechanism. These simulations are not constrained to observations or simulation chamber data. The set-up of the BOXMOX
50 simulations is described in Section 2.1.1. We focus the analysis here on DMS and its major oxidation products and the effects
51 of temperature and [NO_x] on these. Section 3.1 compares DMS mechanisms based around the CS₂ and ST schemes used in
52 UKCA (**Table 1**). In Section 3.2 our newly developed mechanism is compared to other DMS mechanisms from recent literature
53 that also include HPMTF formation.

54 3.1 Comparison of DMS mechanisms used for UKCA

55 3.1.1 Time series analysis

56 The BOXMOX set up allows a quasi steady-state to be achieved for a number of key sulfur species with the main exception
57 being H_2SO_4 , which builds up over time in the model as the model is run without aerosol formation and aerosol microphysics
58 included (**Figure 2**). The DMS concentration simulated with different DMS mechanisms used in UKCA is simulated to be
59 very similar throughout all model runs; the small variations stem from different oxidant concentrations or small differences in
60 the rate constants used for the initiation reaction in the different mechanisms (**Figure 2a**). For instance, the ST run has higher
61 DMS concentration because the NO_x concentration is lower (as is OH) and less DMS is oxidised.

62 The SO_2 concentration is increased and MSA is significantly decreased in the updated CS2 runs (CS2-HPMTF and CS2-UPD-
63 DMS) compared to CS2 (**Figure 2b,c**). Comparing CS2-HPMTF and CS2-UPD-DMS, we can see that this pattern (increased
64 SO_2 and decreased MSA) is due to reaction 7c, which directly forms SO_2 and suppresses CH_3SO_2 , consequently lowering
65 MSA formation. The SO_2 concentration is lower in CS2-HPMTF compared to CS2-UPD-DMS because the addition of
66 HPMTF produces OCS which acts as a long-lived sulfur reservoir. While MSA concentration is very similar between CS2 and
67 ST, SO_2 concentration is not. This is primarily explained through the difference in the treatment of MSA and SO_2 production
68 in CS2 and ST. MSA is not treated as a reactive species in CS2 and ST (in so much as there are no further reactions of MSA
69 after its production). In ST and ST~CS2, 100% of DMS yields SO_2 , regardless of the amount of MSA production. However,
70 as more MSA is produced in CS2 the SO_2 yield is lowered. In spite of higher SO_2 concentrations in the ST DMS schemes, this
71 trend does not translate to H_2SO_4 concentration (**Figure 2d**). SO_2 is a relatively long-lived species (~2 days in our model but
72 with a range from 0.5-2.5 days (Lee et al., (2011))) and can therefore be lost through the mixing processes with the background
73 air in the BOXMOX setup. In CS2, CH_3SO_3 decomposition provides a direct pathway to H_2SO_4 production. In the updated
74 CS2 schemes (CS2-UPD-DMS and CS2-HPMTF) SO_3 production with instantaneous transformation to H_2SO_4 is included.
75 The slower rate constant in CS2 for the decomposition of CH_3SO_3 (11b_old) is compensated by a higher production of CH_3SO_3 .



76
77
78
79
80
81

Figure 2: BOXMOX-simulated gas-phase concentrations as a function of time for a selection of species simulated with the different DMS gas-phase oxidation schemes used in UKCA configurations (oxidation by OH and NO₃). Grey areas denote nighttime, when no photolysis reactions are taking place. Average NO_x concentration is approximately 10 ppt, with an average temperature of 293 K (range: 289 – 297 K).

82 3.1.2 Sensitivity of UKCA DMS schemes to temperature

83 As described in Section 2.1.1, a series of BOXMOX experiments were performed perturbing the temperature profile in the
84 model (**Figure 3**).

85
86 As temperature increases in the box model, the steady-state DMS concentration increases in all simulations. This is mainly
87 because the DMS oxidation by OH addition is negatively temperature dependent. For most models, DMS concentration
88 increases by 85-93 ppt throughout the temperature range from 260 K to 310 K, except the ST run where at temperatures over
89 290 K, a stronger increase of DMS concentration is found, with a total increase of 106 ppt. This could be due to different

90 oxidant concentrations in the model runs using the ST mechanism and independent of the DMS scheme since this stronger
91 increase is not found with CS2-ST.

92 Although the kinetics, and therefore temperature dependence, of DMS loss is comparable across the different schemes, the
93 dependence of MSA and SO₂ on temperature differ significantly.

94

95 Most MSA is formed from the OH-addition channel, which is favoured at low temperatures (Barnes et al., 2006). Therefore,
96 the MSA concentration is higher at lower temperatures across all the UKCA DMS schemes considered (**Figure 3b**). In the ST
97 schemes (ST and ST~CS2), MSA decreases by around 88% (-189 ppt and -197 ppt) throughout the temperature range
98 considered, while in all the CS2 schemes MSA is shown to be much more sensitive to temperature, decreasing by >96% (CS2:
99 -300 ppt, CS2-UPD-DMS: -222 ppt, CS2-HPMTF: -222 ppt) between 270 to 290 K. We attribute this to differences in the
00 rate constant of DMS oxidation through the OH-addition channel (see **Table 2** and **S1.4.1**) used in the UKCA ST schemes and
01 the UKCA CS2 schemes. The expression used in the ST family of schemes (the provenance of which is Pham et al. (1995),
02 see S1.4.1) has a much shallower gradient with temperature than the expression used in the CS2 family of schemes (which is
03 based on the latest IUPAC recommendation). The average MSA concentration for the UKCA schemes diverges most in the
04 temperature range between 270 - 300 K.

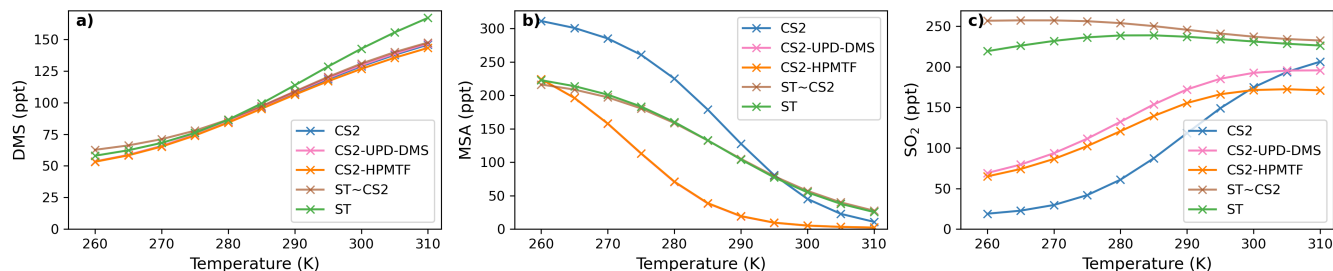
05

06 The difference in SO₂ concentrations between the CS2 schemes and ST schemes are greatest at lower temperature (**Figure**
07 **3c**), with the ST and CS2-ST schemes simulating ~ 5 times (+200 ppt) the SO₂ that is simulated in the other schemes based
08 around CS2. In the ST schemes SO₂ concentration either stays at a similar level across the whole temperature range (ST: +3%)
09 or slightly decreases (ST~CS2: -9%). Conversely, the CS2 family of schemes show a positive temperature dependence (i.e.,
10 $+\frac{d[X]}{dT}$), across the temperature range, especially in the range of relevant atmospheric temperatures from 270 to 290 K. SO₂
11 increases by 298% in CS2, 84% in CS2-UPD-DMS and 79% CS2-HPMTF. In the CS2 schemes, more DMS reacts through
12 the addition pathway which favours the production of MSA, instead of SO₂ therefore reducing the SO₂ concentration. In ST,
13 the addition pathway still leads to 100% SO₂ formation, making the average SO₂ concentration less dependent on temperature.
14 Experimental findings (Arsene et al., 1999) and field measurements (Sciare et al., 2001) both show a positive temperature
15 dependence of SO₂ concentration. This trend is only reproduced by the DMS schemes based on the CS2 mechanistic features
16 (i.e. not the very simple mechanism used in ST), indicating that the ST DMS chemistry is likely insufficient to explain
17 laboratory and field observations, particularly in cold environments and under climate change.

18

19 In these box model experiments only gas phase losses and mixing of species with background air are considered. Under the
20 conditions of our simulations, we find that the MTMP isomerization pathway mainly yields SO₂, as does the rest of the
21 abstraction pathway. Therefore, the addition of the isomerization branch does not have a significant impact on the temperature

22 dependence of SO₂ concentration (comparing CS2-UPD-DMS and CS2-HPMTF), even though the isomerization step itself is
23 greatly temperature dependent.



24
25 **Figure 3:** Temperature dependence of average a) DMS, b) MSA, and c) SO₂ concentration after a quasi steady-state is reached
26 in the box model simulations using the DMS schemes for UKCA.
27

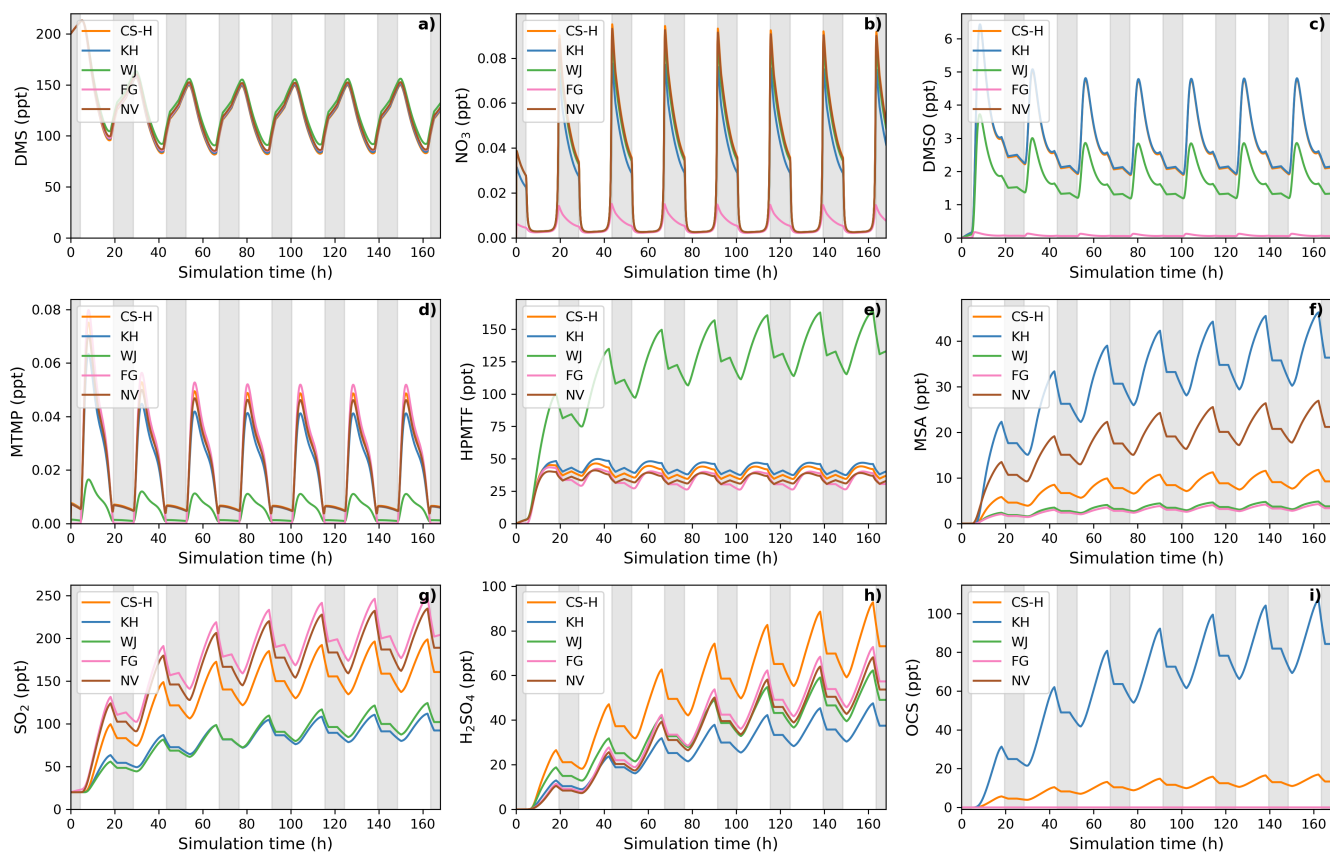
28 3.2 Comparison with DMS schemes that include HPMTF from the recent literature

29 Here, four recently published DMS schemes that also include the isomerization pathway and formation of HPMTF are
30 compared with our new mechanism, CS2-HPMTF (*CS-H*, 36 reactions in DMS scheme), as follows. To make the studies
31 comparable, only DMS oxidation by NO₃ and OH and gas-phase reactions are considered. The implementation of these
32 chemical schemes in BOXMOX can be found in the *Supporting Information S1.3*.

- 33 • *Fung et al. (2022) (FG)*: This scheme includes 32 reactions for the DMS oxidation chemistry. The H-abstraction
34 pathway is based on the MCM, while the rate constants in the OH-addition pathway mostly stem from Burkholder et
35 al. (2015) or a scaled up version of those. The rate constant of MTMP isomerization to HPMTF is based on Veres et
36 al. (2020).
- 37 • *Wollesen de Jonge et al. (2021) (WJ)*: This scheme is the most complex and consists of 98 reactions, including
38 reactions from the MCM and from Hoffmann et al. (2016). The isomerization branch mostly uses the rate constants
39 by Wu et al. (2015), except the first isomerization rate constant, which is a combination of Veres et al. (2020) and
40 Berndt et al. (2019).
- 41 • *Khan et al. (2021) (KH)*: This scheme is based on Khan et al. (2016), which is equivalent to the DMS chemistry in
42 CS2 (CRI v2 R5). The mechanism was modified to include the isomerization pathway and photolysis loss and
43 temperature dependent OH oxidation of HPMTF by the authors. In total, the DMS chemistry consists of 38 reactions,
44 5 of which are photolysis reactions.
- 45 • *Novak et al. (2021) (NV)*: This is a simplified scheme that aims to only include the intermediates necessary for
46 HPMTF formation and consists of only 10 reactions. DMS therefore either directly yields MSA (without DMSO
47 formation) or first forms MTMP, which isomerizes to form HPMTF or is oxidised to SO₂.

49 Using this ensemble of gas-phase DMS oxidation schemes in BOXMOX simulations leads to significant differences in the
 50 concentrations of important oxidation intermediates and products, even though DMS concentration is similar across all models
 51 (**Figure 4**).

52 3.2.1 Time series analysis of different DMS-HPMTF schemes



53
 54 **Figure 4:** Gas-phase concentrations as a function of time for different DMS gas-phase oxidation schemes (oxidation by OH
 55 and NO₃). Average NO_x concentration is approximately 10 ppt, with an average temperature of 293 K (range: 289 – 297 K).
 56 Grey areas denote nighttime when no photolysis reactions are taking place.

57
 58
 59 The depletion of DMS due to OH and NO₃ oxidation is similar across most models (**Figure 4a**) since the major oxidants are
 60 relatively constrained by the box model experiment set up (see Section 2.1.1) and they mostly rely on IUPAC or JPL
 61 recommended values (Atkinson et al., 2004; Burkholder et al., 2015). One exception is NO₃ oxidation in the FG scheme, which
 62 uses a rate constant a factor of approximately 6 higher than the JPL recommendation. On the one hand, this does not affect
 63 DMS concentration, since OH oxidation of DMS plays a greater role, on the other hand, the concentration of NO₃ in the FG

64 scheme's simulation run is controlled by the greater NO₃ oxidation rate (**Figure 4b**). WJ includes the intermediate
65 CH₃S(OH)CH₃ and its decomposition back to DMS (based on Hoffmann et al., (2016)), which in their experiments improved
66 the fit between their measured and modelled DMS concentration. Here, this does not have any significant impact on DMS
67 concentration, compared to all the other schemes.

68
69 Significant differences between the models can be found for the DMSO concentration (**Figure 4c**). KH and CS-H have the
70 highest DMSO concentration since all DMS that is oxidised through the OH-addition pathway yields DMSO. This is not the
71 case for WJ, where CH₃SOH and to a small part DMSO₂ are also possible products. In the FG simulation, DMSO concentration
72 is close to zero, which is due to a much faster loss of DMSO; a rate constant a factor of 15 faster than experimental
73 measurements by Urbanski et al. (1998). NV does not include DMSO as an intermediate. Since the lifetime of DMSO was
74 found to be several hours (Urbanski et al., 1998; Ye et al. 2021), deposition of DMSO could act as a significant sink of
75 atmospheric sulfur (as found by Chen et al. (2018)). Fast oxidation of DMSO in FG, or omitting the species in NV, might
76 therefore lead to an over-estimation of other DMS oxidation products in those schemes.

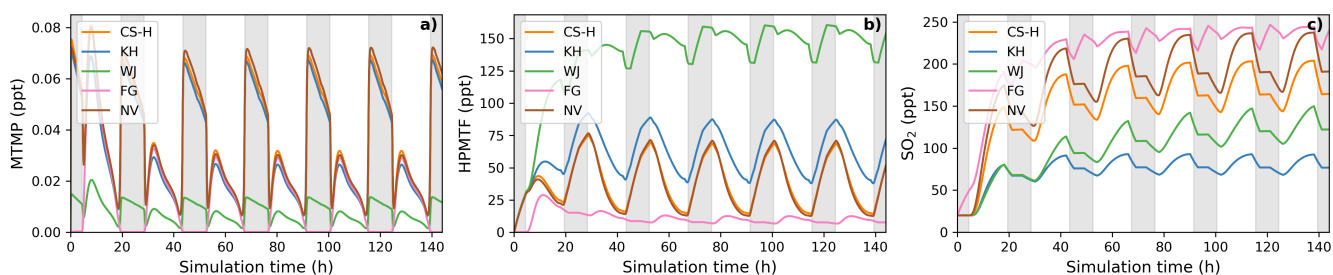
77
78 Regarding the intermediate MTMP, WJ shows the greatest deviation from the ensemble (**Figure 4d**). The MTMP concentration
79 never exceeds 0.02 ppt in WJ, while the other mechanisms simulate concentrations over three times higher. WJ employs a
80 faster isomerization rate constant of MTMP to HPMTF. They scale the A-factor by 5 to get a rate constant that is a combination
81 of the theoretical calculations by Veres et al. (2020) and the experimental findings by Berndt et al. (2019). Additionally, they
82 include more oxidation reactions of MTMP (such as oxidation by NO₃) but since the isomerization to HPMTF already
83 outcompetes most oxidation reactions anyway (>97%), we found them to play a negligible role (<0.1%). In the FG scheme,
84 DMS + NO₃ leads to immediate SO₂ formation, without prior MTMP formation. Therefore, no MTMP is produced during the
85 nighttime, when NO₃ oxidation becomes relevant. Under conditions with low NO_x (around 10 ppt in this experiment) this does
86 not have significant impacts but at higher NO_x concentrations this leads to a major deviation from the other simulations (**Figure**
87 **5a**, 100 ppt NO_x). At night, CS-H, KH, and NV reach MTMP concentrations of 0.07 ppt, allowing nighttime HPMTF
88 formation, while FG stays zero.

89
90 All model simulations, except WJ, are very similar in HPMTF concentration (**Figure 4e**). The fast isomerization rate constant
91 in WJ is one of the reasons HPMTF concentration is on average more than 3 times higher than the other model simulations.
92 The other reason is a much slower oxidation of HPMTF by OH. While most models use a value of (or close to) 1.11×10^{-11}
93 $\text{cm}^3 \text{ molecule}^{-1} \text{ s}^{-1}$, recommended by Vermeuel et al. (2020), WJ use the much slower rate constant calculated by Wu et al.
94 (2015), $1.4 \times 10^{-12} \text{ cm}^3 \text{ molecule}^{-1} \text{ s}^{-1}$. This rate constant is also used in the KH scheme but it additionally includes HPMTF
95 depletion by photolysis which ultimately leads to the similar HPMTF concentration as in CS-H, FG, and NV. The addition of
96 the photolysis reactions in KH does not affect the diel profile of HPMTF, even though those account for 81% of chemical loss
97 of HPMTF in their scheme. It is therefore unlikely that the observed diel profile of HPMTF by Vermeuel et al. (2020) and

98 Khan et al. (2021) can be explained solely by considering loss of HPMTF to aldehyde and hydroperoxide photolysis. Reducing
99 HPMTF formation to one isomerization reaction without any side reactions as is done in this work and NV, does also not affect
00 the diel profile of HPMTF significantly.

01 The effect of higher NO_x conditions on the diel profile of HPMTF varies significantly between the different schemes (10 ppt
02 NO_x in **Figure 4** vs. 100 ppt NO_x in **Figure 5**). Higher NO_x concentration leads to more DMS oxidation by NO₃ at night and
03 the subsequent increase in MTMP concentration and therefore HPMTF concentration during the night hours in the CS-H, WJ,
04 KH, and NV simulations. At low NO_x, HPMTF concentration stayed more or less stable throughout the nighttime and increased
05 in the morning, reaching a plateau in the afternoon, and dropping in the evening (**Figure 4e**). Under higher Nox conditions,
06 HPMTF increases in these mechanisms throughout the night and decreases throughout the day when it is oxidised by OH
07 (**Figure 5b**). In the WJ simulation, the diel profile has more plateaus and small deviances but the overall trend still fits the
08 described pattern. This is not true for FG, where DMS oxidation by NO₃ leads directly to SO₂ formation.

09



10

11 **Figure 5:** BOXMOX simulations where the average NO_x concentration is approximately 100 ppt (a factor 10 greater than for
12 the results presented in **Figure 4**). **(a)** MTMP, **(b)** HPMTF, and **(c)** SO₂ concentration as a function of time for different DMS
13 gas-phase oxidation schemes (oxidation by OH and NO₃). Average temperature of 293 K (range: 289 – 297 K). Grey areas
14 denote nighttime when no photolysis reactions are taking place.

15

16 While the diel profile of MSA looks similar for all simulations, the average concentrations do not (**Figure 4f**). The highest
17 average steady-state MSA concentration is reached in the KH simulation, which is a factor of 10 higher than the lowest average
18 concentration in the FG simulation. In our experimental setup, most of the simulations we performed with the different
19 mechanisms do not include any (significant) gas-phase chemical loss pathway for MSA; MSA is only lost through mixing and
20 transport out of the “box”. Therefore, the concentration of MSA is a direct reflection of MSA production in the respective
21 simulations.

22

23 KH simulates the highest production of MSA (similar to CS₂), where MSA is formed through the addition (MSIA + OH →
24 0.05 MSA + 0.95 CH₃SO₂, reaction 9b,c) and the abstraction channel (CH₃SO + O₃ → CH₃SO₂, reaction 7c_old) of DMS
25 oxidation, with CH₃SO₂ partly being oxidised to CH₃SO₃ and then to MSA (reactions 10b,c, 11a). The decomposition of

26 CH_3SO_3 to H_2SO_4 in KH is slower than in other mechanisms, increasing the branching ratio for MSA formation in their
27 mechanism. In NV, the simulation with the second highest average MSA concentration, the only source of MSA is the direct
28 production of MSA through OH oxidation through the addition channel, where 25% of DMS forms MSA. In both, CS-H and
29 WJ, the abstraction pathway mostly produces SO_2 and only contributes negligible amounts to CH_3SO_2 formation, hence MSA.
30 Similar to KH, the oxidation of DMS through the addition pathway in CS-H and WJ yields CH_3SO_2 of which a part forms
31 MSA. However, not all of the CH_3SO_2 results in MSA, some of it also decomposes to SO_2 or yields SO_3 . This explains the
32 lower concentration of MSA in CS-H and WJ compared with NV. The reason why CS-H has a higher MSA concentration than
33 WJ is because of the inclusion of reaction 9b (**Table 2**), which yields MSA directly and is not part of the WJ scheme.
34 The lowest MSA concentration is found in FG and WJ, where 60% of the OH-addition pathway directly produces SO_2 . Out of
35 the 40% of DMS that forms DMSO in this pathway, only a fraction yields MSA.

36

37 To harmonise the results and aid interpretability, the same rates (based on CS2) are used for the loss processes of SO_2 in all
38 the mechanisms considered here, therefore the concentration of SO_2 can be used as a proxy for SO_2 production, just as for
39 MSA. The highest SO_2 concentration can be seen in schemes that have the smallest number of intermediates or the most direct
40 pathways from DMS to SO_2 , in NV and FG (**Figure 4g**). Fewer intermediates result in less opportunities for the formation of
41 side products or less long-lived species that can be lost through transport or deposition. For instance, in WJ HPMTF is lost
42 through mixing with the background before it can form SO_2 . Likewise, KH has a higher ratio of MSA and OCS production,
43 which lowers the SO_2 yield. The diel profile of SO_2 concentration is in most simulations not affected by higher NO_x
44 concentrations, with the general trend being an increase of SO_2 concentration during the day and a decrease at night (**Figure**
45 **5c**). The only exception is the FG simulation, where we see a clear increase through part of the night, due to the reaction DMS
46 $+ \text{NO}_3 \rightarrow \text{SO}_2$.

47

48 The H_2SO_4 concentration is influenced by SO_2 production and CH_3SO_3 production and the rate of decomposition of SO_3 to
49 H_2SO_4 . CS-H has the highest average H_2SO_4 concentration and KH the lowest; all other models are very similar to each other
50 (**Figure 4h**). In general, higher SO_2 concentration leads to more H_2SO_4 , since SO_2 is first oxidised to SO_3 and then to H_2SO_4
51 with the same rates across all schemes. However, all models except NV include an additional pathway of H_2SO_4 formation: in
52 KH and FG, H_2SO_4 is directly formed from CH_3SO_3 , while in CS-H and WJ CH_3SO_3 decomposes to SO_3 first, which then
53 instantly reacts to H_2SO_4 . In KH, the rate constant for the decomposition of CH_3SO_3 at 295 K is a factor of 15 slower than in
54 the other models. Since the SO_2 concentration is also relatively low, it explains why KH has the lowest H_2SO_4 concentration
55 of all schemes when reaching steady-state. CS-H results in a higher H_2SO_4 concentration than FG or NV even though those
56 models have a higher SO_2 concentration. The reason is a higher production of CH_3SO_3 that is then decomposed to SO_3 and
57 H_2SO_4 .

58

59 Similar to the other products of the DMS scheme, the concentration of OCS is a reflection of its production. OCS is only
60 produced from oxidation of HPMTF by OH and, in the KH scheme, through photolysis of HPMTF. In KH, 60% of HPMTF
61 forms OCS, resulting in the highest OCS concentration (**Figure 4i**). This stems mainly from the large contribution of the
62 photolysis reactions. Potentially, the rate constant of OH oxidation of HPMTF in KH is too low and therefore OCS might be
63 overestimated. In CS-H, 10% of HPMTF is oxidised to OCS, resulting in an OCS concentration that is on average 5.5 times
64 lower than KH. FG and WJ both use the theoretically determined branching ratio by Wu et al. (2020), which results in only
65 0.007% of HPMTF being oxidised to OCS at 295 K. NV does not include this pathway. Very recent evidence suggests that
66 there is a small (2%) but prompt source of OCS following the formation (and decomposition) of HPMTF as well as a significant
67 OCS yield (13%) from the HPMTF + OH reaction (Jernigan et al., 2022). These new data were not assessed (or included) in
68 this work but we estimate that inclusion of these mechanistic pathways would result in OCS yields higher than CS-H and the
69 other mechanisms (which have used a very small yield in the past) but consistently lower than that simulated by KH.
70 To summarise, the intercomparison of recent gas-phase DMS oxidation mechanisms complements and extends earlier studies
71 on DMS (Karl et al., 2007). Recent gas-phase DMS oxidation schemes used in modelling studies lead to a wide range in results
72 of key DMS oxidation products, with moderate Nox levels (~ 0.1 ppb) leading to greater divergence than low Nox levels (~
73 10 of ppt). A similar situation was found for isoprene by Archibald et al. (2010) and significant efforts have been employed to
74 improve our understanding of isoprene oxidation through theoretical and laboratory experiments (e.g., Jenkin et al., 2015;
75 Wennberg et al., 2018). We now focus on the role of temperature on the divergences seen thus far.

76

77 **3.2.2 Temperature dependence of different DMS-HPMTF schemes**

78 **Figure 6** shows that even though the temperature dependence of average DMS concentration is similar across all schemes, the
79 temperature dependence of average SO₂ and MSA concentration differs from scheme to scheme significantly. Most of the
80 general trends were found to be similar and in line with the trends observed for the UKCA schemes and have been explained
81 there (Section 3.1.2, **Figure 3**).

82

83 While WJ has the highest absolute change in HPMTF concentration throughout the temperature range (+131 ppt, +380%;
84 **Figure 6b**), CS-H, KH, and NV show higher relative change (+43-48 pp, +763-892%). Since FG is missing the DMS oxidation
85 by NO₃ as a potential pathway to HPMTF (via MTMP), HPMTF in FG is least affected by temperature (+34 ppt, +256%).

86

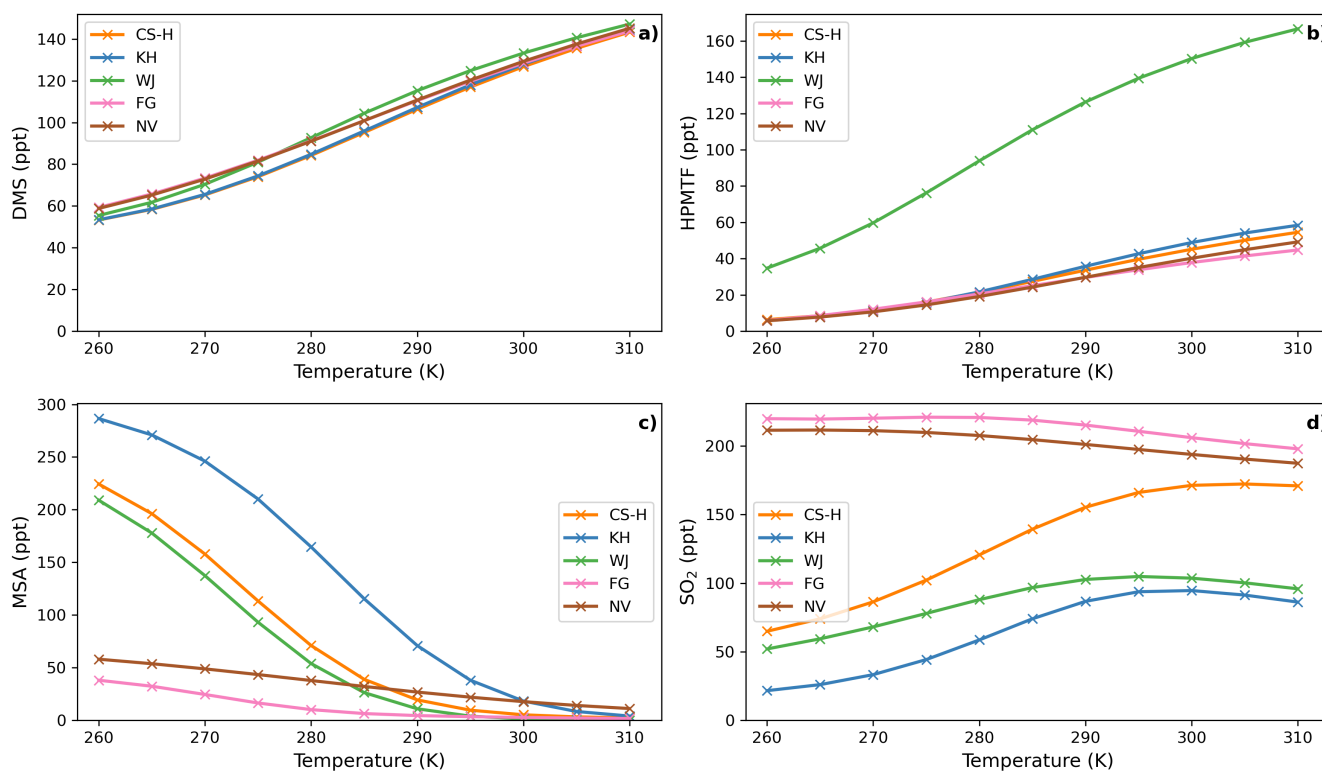
87 MSA is even more affected by temperature than HPMTF (**Figure 6c**). Its concentration shows a strong negative temperature
88 dependence in all simulations (**Figure 6c**). The magnitude of MSA-temperature dependence differs from scheme to scheme.
89 The smallest changes can be observed in NV (-47 ppt from 260 – 310 K), where only 25% of DMS that is oxidised through
90 the OH-addition pathway forms MSA. Similarly in FG (-67 ppt from 260 – 310 K), where only 40% of the OH-addition

91 pathway forms DMSO and then potentially MSA. The largest temperature dependence can be found in the KH simulation,
92 with a change of MSA concentration of -282 ppt from 260 K to 310 K, which is very similar to CS2 (**Figure 3c**).

93

94 In almost all schemes, SO₂ concentration increases with temperature (**Figure 6d**). The greatest positive change happens
95 between the atmospheric relevant temperatures 270 and 290 K. KH and CS-H show the greatest increase in this temperature
96 range with +53 ppt (+160%) and +69 ppt (+80%), respectively (WJ: +34 ppt (51%)). Starting at 295 K, SO₂ concentration
97 plateaus with further increasing temperature and even declines slightly in some simulations (Figure 6d). NV and FG are the
98 only models which show a decrease in SO₂ throughout the entire temperature range of 260 – 310 K (NV: -24 ppt, -11%, FG:
99 -22 ppt, -10%), similar to ST~CS2 in **Figure 2d**. This could be due to previously mentioned simplifications in the DMS
00 additional channel, where DMSO is either completely omitted or rapidly oxidised further.

01



02

03 **Figure 6:** Temperature dependence of average (a) DMS, (b) HPMTF, (c) MSA, and (d) SO₂ concentration in different DMS
04 oxidation schemes after a quasi steady-state is reached in the box model simulation. Average Nox is approximately 10 ppt.

05

06 These results demonstrate limited consensus on gas-phase DMS oxidation, similar to the earlier work of Karl et al., 2007.
07 Importantly in the context of the role of DMS in chemistry-aerosol-climate feedbacks, we have further shown that this

08 uncertainty across mechanisms is amplified when assessing temperature sensitivity of the products of DMS oxidation. Small
09 uncertainties in the rate of reactions or the omission of intermediates can have significant effects on the resulting product
10 concentrations, as we have shown through our systematic work updating the CRI-Strat DMS scheme. All models studied tend
11 to agree on the rates of oxidation of DMS, largely controlled for by the fairly uniform treatment of the initial oxidation step.
12 However, we saw (in Figure 5) that there is large divergence at high No_x levels for MTMP and subsequently HPMTF and
13 SO_2 . In part this divergence could be reduced by better constraining the MTMP self- and cross-reactions, but in the case of
14 Fung et al. (2022) including MTMP as a product of the $\text{NO}_3 + \text{DMS}$ reaction would help it converge with the other models.
15 The effects of climate change are that it is likely that global mean surface temperature will remain higher than the pre-industrial
16 baseline for some time to come. As a result, the simulations would all suggest an increase in the amount of HPMTF formed
17 relative to other major oxidation products, especially, MSA, and most likely an overall increase in SO_2 . However, our box-
18 modelling study highlights how uncertain the situation is within the context of the current literature. At present there is a need
19 for more laboratory data and more focused sensitivity studies to isolate the major sources of uncertainty that are common
20 across DMS oxidation mechanisms and constrain them. Strikingly we see that the ST and CS2 mechanistic variants used for
21 UKCA studies span the wide range of SO_2 -Temperature and MSA-Temperature sensitivities as the recently reported updated
22 DMS mechanisms. We now move on to discuss our work implementing the CS2-H mechanism into our global chemistry-
23 climate model.

24 **4 Results from 3D model simulations using UKCA**

25 Here we present our results from the incorporation of the new CS2-H DMS mechanism described above in the 3D UKCA
26 chemistry climate model. As described in Section 2.1, we performed a series of 12-month nudged simulations with UKCA for
27 the year 2018 using 6 model simulations, with different mechanistic variants (**Table 1**). As a reminder, we use the CS2
28 simulation (Archer-Nicholls et al., 2021) as the “base” simulation, to which mechanistic improvements are made. More details
29 can be found in the SI in Section 2.

30 **4.1 Distribution of key sulfur species (DMS, HPMTF, SO_2 and sulfate).**

31 The annual mean global DMS burden was found to be between 63-66 Gg S in all model simulations. DMS concentration
32 follows a seasonal modulation with maximums in the warmer months, which coincide with phytoplankton blooms (See the SI
33 **Fig. S6a**). **Figure S6b** and **S6c** show the annual mean vertical profiles in the central North Atlantic region and the Southern
34 Ocean (see figure caption for bounding areas). These regions are focused on owing to the differences shown in the mixing
35 ratios of key species and the importance of these two regions to global climate (e.g., Sutton et al., 2018; Caldeira and Duffy
36 2000). In the Southern Ocean, DMS mixing ratios vary between 100 and >300 ppt. On the other hand, in the North Atlantic
37 region analysed, DMS concentrations rarely reach over 50 ppt. Here, <1 ppt DMS is found above the boundary layer (above
38 1000 m), while in the Southern Ocean DMS decreases more slowly up-to the tropopause (~8000 m). These differences in DMS

39 distribution are a complex function of the local heterogeneity of the DMS source from the ocean and differences in the lifetime
40 of DMS due to different simulated cloud and oxidising environments (with the North Atlantic generally being a region of
41 greater oxidising capacity than the Southern Ocean (Archer-Nicholls et al., 2021; Griffiths et al., 2021))

42

43 There is a significant bias in the simulated DMS mixing ratios compared with observations, which we note has been seen in
44 several other modelling studies (e.g., Fung et al. (2022)) and is driven not by the DMS chemistry but by the oceanic emissions,
45 in our case by the bias in the UKESM derived DMS emissions field (Bhatti et al., 2023). See the SI for further details.

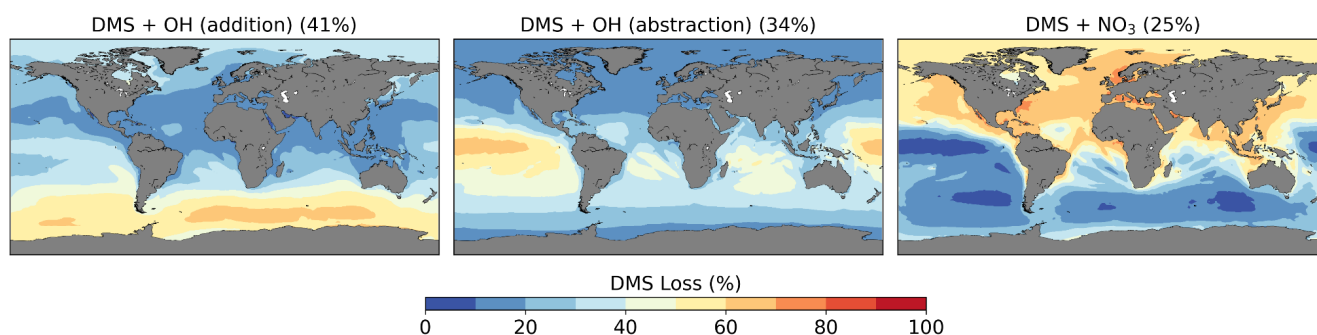
46

47

48 4.1.1 Oxidation of DMS

49 We calculate a global average tropospheric lifetime of 1.5 days for DMS. **Figure 7** shows the global distribution of the different
50 DMS oxidation pathways in the base run (these results are not affected by the different DMS mechanism variants we use as
51 these reactions were not updated and there is only a weak feedback of DMS oxidation products on DMS oxidation itself). 75%
52 of DMS is oxidised by OH (41% via the OH-addition channel and 34% via the H-abstraction channel) and 25% by NO₃.
53 Oxidation by NO₃ is dominant in the Northern Hemisphere, especially close to the coast and over ship routes. In the Southern
54 Hemisphere, where DMS emissions are highest, the contribution is less than 20%. The addition pathway of OH oxidation is
55 favoured at lower temperatures, explaining the trend of higher DMSO formation at high latitudes.

56



57

58 **Figure 7:** Spatial distribution of mean percentage of DMS oxidation via DMS + OH (addition), DMS + OH (abstraction), and
59 DMS + NO₃ in the CS2 base run. The percentage in brackets denotes the contribution of this channel to the global chemical
60 loss of DMS. Only values above the ocean are shown.

61

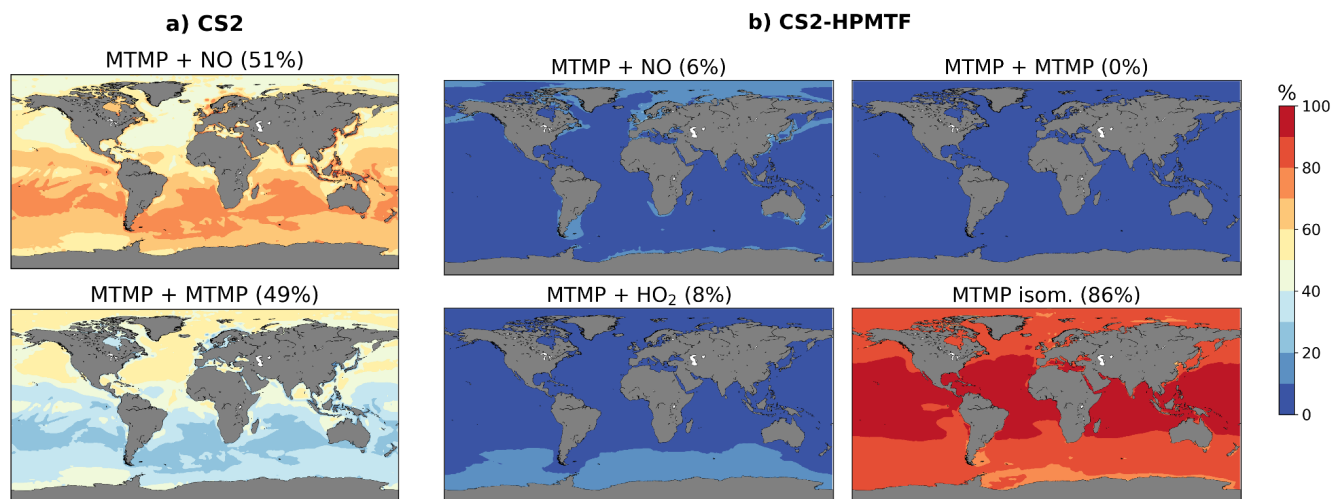
62

63

64 4.2 DMS Oxidation products

65 59% of DMS forms MTMP, the first intermediate of the abstraction pathway. In CS2, MTMP is oxidised by NO (51%) or
66 reacts with itself (49%) to form CH₃S (**Figure 8a**) which is further oxidised to SO₂, H₂SO₄, and MSA. This is clearly wrong
67 and a failure of the CS2 scheme. With the updates implemented in CS2-HPMTF, 86% of MTMP isomerizes to HPMTF, while
68 8% is oxidised by HO₂, and only 6% by NO (**Figure 8b**). The self-reaction becomes negligible with the additional loss
69 processes of MTMP, significantly lowering MTMP concentrations. The global tropospheric lifetime of MTMP is reduced from
70 26 min to less than one minute.

71



72

73 **Figure 8:** Spatial distribution of annual mean percentage of MTMP depletion (< 2 km) via MTMP + NO, its self-reaction,
74 MTMP + HO₂, and isomerization to HPMTF in **a) CS2** and **b) CS2-HPMTF**. The percentage in brackets denotes the
75 contribution of this channel to the global chemical loss of MTMP. Only values above the ocean are shown.

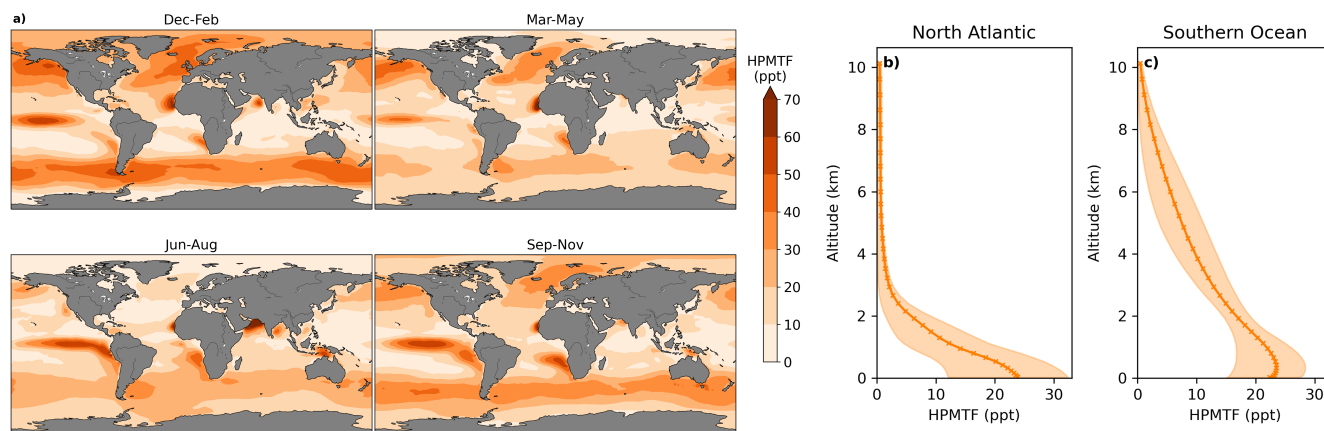
76

77

78 4.2.1 Modelled HPMTF

79 In CS2-HPMTF 51% of DMS forms HPMTF. The general patterns of the global distribution of HPMTF are similar to those
80 of DMS in **Figure 9**, except that relatively higher concentrations of DMS are reached in the Southern Ocean. There,
81 temperatures are lower and therefore the OH-abstraction pathway, as well as the strongly temperature-dependent isomerization
82 reaction from MTMP to HPMTF are disfavoured. At the surface, the annual mean HPMTF concentration is similar in the
83 North Atlantic and the Southern Ocean with approximately 20 ppt. However, in the North Atlantic, the variability throughout
84 space and time is greater (bigger interquartile range). Further, the vertical profiles differ visibly: In the North Atlantic HPMTF
85 concentration decreases in the boundary layer and above 2500 m HPMTF concentration is virtually zero (**Figure 9b**). In the

86 Southern Ocean, the concentration decreases more slowly and only reaches zero at 10000 m (**Figure 9c**). The HPMTF burden
87 in CS2-HPMTF is 24 Gg S and HPMTF has a lifetime of 26 hours
88



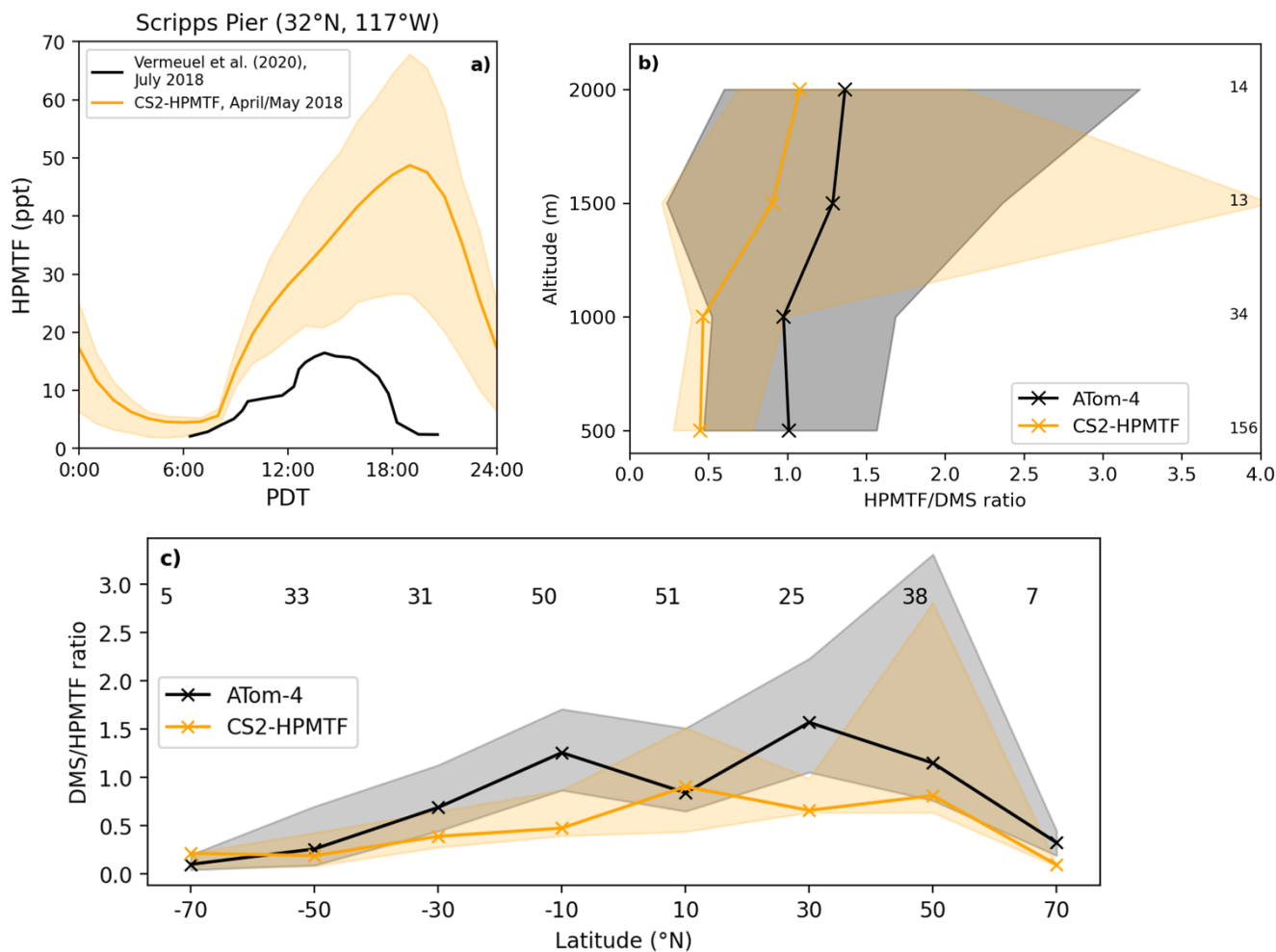
89
90 **Figure 9:** Seasonal average **a)** Global distribution of HPMTF mixing ratios in the lower troposphere (< 2 km) over the ocean
91 in CS2-HPMTF. Annual means of the vertical distribution of HPMTF are shown in **b)** the Central North Atlantic (30-50°E,
92 20-45°N) and **c)** the Southern Ocean (50-70°S). The envelopes represent the interquartile range of the model data.

93

94 **Comparison of HPMTF with observations**

95 Since DMS in the model is likely overestimated, the same would be expected for HPMTF. **Figure 10a** shows that the
96 implemented loss processes in CS2-HPMTF already lead to a diel profile of HPMTF that is similar to the one measured by
97 Vermeuel et al. (2020) (where no DMS measurements were made), without the need to add aqueous loss or photolysis. While
98 DMS at low altitudes was overestimated by a factor of 5 in the model (see SI), the maximum HPMTF is only 3.7 times higher
99 than the highest measurement in the diel profile at Scripps Pier (**Figure 10a**). For the comparison with ATom-4 data (**Figure**
00 **10b,c**), the DMS/HPMTF is used to account for the discrepancy between DMS concentrations observed and in the model. The
01 model generally underestimates the HPMTF/DMS ratio. For instance, up until 1000 m, the ratio in the model is half of the
02 measured ratio. These results indicate that loss processes of HPMTF might still be too fast in the model or the oxidation of
03 DMS too slow. The CS2 oxidants have been evaluated before (Archer-Nicholls et al., 2021) and were found to be higher in
04 the boundary layer than in ST simulations used in CMIP6 studies but well within the spread of other models (Griffiths et al.,
05 2021; Stevenson et al., 2020).

06



07
08 **Figure 10: a)** Comparison of the diel profile of HPMTF at the Scripps Pier at the California Coast (32°N, 117°W). The
09 observational data (Vermeuel et al., 2020) is the mean of measurements from July 26 to August 3, 2018, while the model
10 output is the mean from April/May 2018. **(b)** Vertically binned (500 m) and **(c)** latitudinally binned (20°) median
11 DMS/HPMTF ratio along the ATom-4 flight path. The envelopes represent the interquartile range of the measurements and
12 the respective model results while the numbers on the side/on top give the number of measurements in the respective bin.

13

14 4.2.2 Modelled SO₂ and sulfate

15 In CS2-HPMTF the SO₂ burden is increased by 5.6% compared with CS2, to 391 Gg S (**Table 4**). While this percentage seems
16 low, a significant contribution to the SO₂ burden stems from anthropogenic sources and is mainly located above the land. The
17 increase of SO₂ over the remote ocean, especially over the Southern Ocean, can reach up to 400% (**Figure S12**). At high

18 latitudes, the new chemistry implemented in CS2-HPMTF also introduces a stronger seasonality to SO₂, whereby SO₂
19 concentration is higher in respective warmer months than in CS2 (**Figure S11a, Figure S12**). Comparison of CS2-HPMTF
20 with ST reveals that the SO₂ burden is 9.2% higher in the ST run, which uses a 100% SO₂ yield from DMS (**Figure S9** in the
21 SI). The global annual tropospheric sulfate burden is increased in CS2-HPMTF by 3.7% compared with CS2, to 604 Gg S.
22 However, the sulfate burden is 5.3% higher in ST than in CS2-HPMTF (**Table 4**).

23
24
25

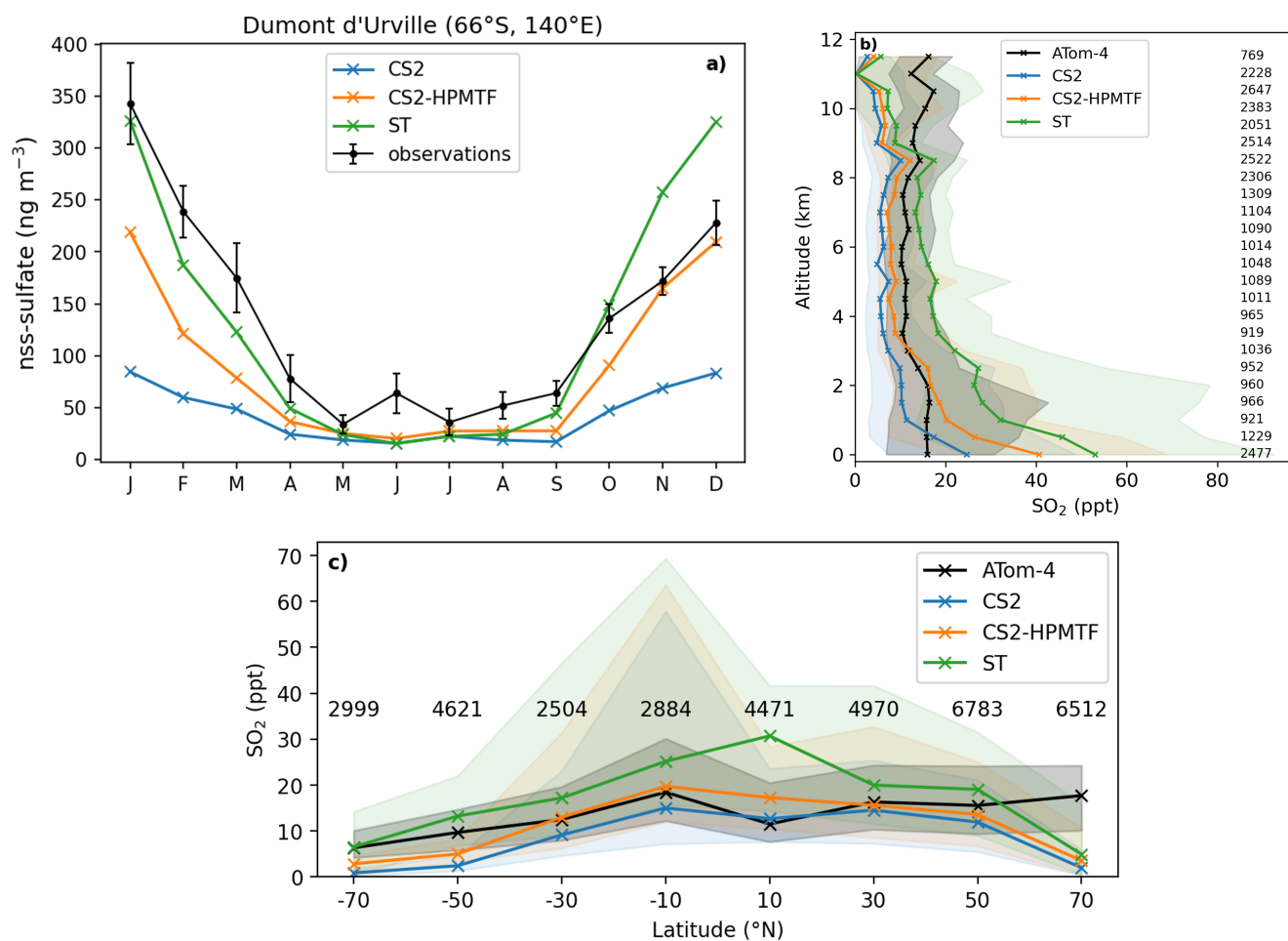
26 **Comparison to observed SO₂ and sulfate**

27 **Figure 11a** shows the monthly means of observed non-sea-salt sulfate (nss-sulfate) concentration at Dumont d'Urville station
28 (66°S, 140°E) between 1991 and 1995 (Minikin et al., 1998) and compares it to the sulfate concentration in the three different
29 UKCA model runs. The seasonal changes in sulfate concentrations are reproduced by CS2-HPMTF and ST, but not by CS2.
30 From April to September all three runs match the observations adequately well. Earlier in the year, the results from the ST run
31 match the observations best, while later in the year CS2-HPMTF reproduces the measurements better.

32

33 **Figure 11b,c** show SO₂ measurements along the ATom-4 flight path in comparison with the modelled SO₂ concentrations. In
34 the boundary layer, all runs over-predict SO₂ in comparison to the ATom-4 data (**Figure 11b**). In addition to wet and dry
35 deposition (Faloona 2009; Ranjithkumar et al., 2021), vertical mixing has been identified as a major source of uncertainty in
36 models (Gerbig et al., 2008) and could provide an explanation for the mismatch between the simulation results and
37 observations. At altitudes above 1.8 km, CS2-HPMTF is able to reflect SO₂ concentrations better than the other schemes.
38 Above 9 km, the simulations underestimate SO₂, potentially indicating issues with convective transport. Overall, in the ATom-
39 4 observations, SO₂ stays broadly constant with altitude, suggesting significant secondary sources or efficient vertical transport,
40 while in the simulations it decreases. Additionally, the interquartile ranges of the concentrations in each bin are bigger,
41 indicating a greater variance of model results than measured values. Overall, the mean SO₂ concentrations by the models in
42 each latitude bin predict the mean observation values well (**Figure 11c**). However, the variation of values is again greater in
43 the model, especially at low latitudes. The underestimation of SO₂ at 70°N could be due to an underestimation of the influence
44 of anthropogenic SO₂ emissions or unrealistic deposition of SO₂ (Hardacre et al., 2021). Alternatively, the SO₂ production
45 from DMS might be too slow still.

46



48

49 **Figure 11: a)** Comparison of nss-sulfate concentration at the Dumont d'Urville Station (66°S, 140°E) at the coast of Antarctica.
 50 The observational data stems from Minikin et al. (1998) and represents the monthly mean concentrations and their standard
 51 deviations for the years 1991-1995. **(b)** Vertically binned (500 m) and **(c)** latitudinally binned (20°) median SO_2 mixing ratio
 52 along the ATom-4 flight path. The envelopes represent the interquartile range of the measurements and the respective model
 53 results while the numbers on the side/on top give the number of measurements in the respective bin.

54

55

56 4.3 Sensitivity runs

57 To improve our understanding of the variability of the model results, based on the uncertainties of HPMTF formation and loss,
 58 three sensitivity runs were conducted (CS2-HPMTF-CLD, CS2-HPMTF-FL, CS2-HPMTF-FP, **Table 1**). Loss of HPMTF to

clouds was proposed to be a major loss pathway by Veres et al. (2020) and Vermeuel et al. (2020). CS2-HPMTF-CLD adds cloud and aqueous uptake of HPMTF with a reactive uptake coefficient, γ , of 0.01, used in the study by Novak et al. (2021). Jernigan et al. (2022) recently established a rate constant for oxidation of HPMTF by OH as $1.4 (0.27\text{--}2.4) \times 10^{-11} \text{ cm}^3 \text{ molecule}^{-1} \text{ s}^{-1}$ through constrained chamber modelling using a rate constant for the formation of HPMTF as 0.1 s^{-1} . Ye et al. (2022) also measured the rate constant for this reaction. In their study they derived a rate constant of $2.1 \times 10^{-11} \text{ cm}^3 \text{ molecule}^{-1} \text{ s}^{-1}$ and an isomerization rate constant, k_{isom} , of $0.13 \pm 0.03 \text{ s}^{-1}$ at 295 K. Whilst, further laboratory studies would be helpful in constraining the rate constant for OH + HPMTF, we recommend future work go into constraining the products of this reaction. Vermeuel et al. (2020) found the theoretically calculated rate constant $1.4 \times 10^{-12} \text{ cm}^3 \text{ molecule}^{-1} \text{ s}^{-1}$ by Wu et al. (2015) too slow and proposed a rate constant of $1.11 \times 10^{-11} \text{ cm}^3 \text{ molecule}^{-1} \text{ s}^{-1}$ instead, based on structurally similar molecules and modelling of their ground-based observations, similar to what we used in CS2-HPMTF. They recommend an upper limit of $5.1 \times 10^{-11} \text{ cm}^3 \text{ molecule}^{-1} \text{ s}^{-1}$ for the HPMTF+OH rate constant. Khan et al. (2021) and Novak et al. (2021) use $5.5 \times 10^{-11} \text{ cm}^3 \text{ molecule}^{-1} \text{ s}^{-1}$ for sensitivity tests, which was also employed in CS2-HPMTF-FL. Further, the study by Ye et al. (2021) looked at the uncertainty of the HPMTF isomerization rate. They estimate the isomerization rate constant as 0.09 s^{-1} ($0.03\text{--}0.3 \text{ s}^{-1}$, $1\sigma_g$ geometric standard deviation at 293 K). Veres et al. (2020) are on the lower end of this range (0.041 s^{-1}) and Berndt et al. (2019) at the higher end (0.23 s^{-1}). The CS2-HPMTF-FP simulation scales the rate constant of Veres et al. (2020) by a factor of 5 to match Berndt's measurements at 295 K to examine the effects of higher HPMTF production. This rate constant was also used by Wollesen de Jonge et al. (2021) in their study. The annual mean of global tropospheric burdens of relevant species in these sensitivity runs are compared in **Table 4**.

77

Table 4: Global annual mean tropospheric burdens of atmospheric sulfur species in UKCA base and sensitivity runs (first half of the table) and comparison to literature values (second half of the table, same acronyms as in Section 3)

79

Run	HPMTF burden (Gg S)	SO ₂ burden (Gg S)	Sulfate burden (Gg S)
CS2	-	370.1	582.3
ST	-	469.7	635.9
CS2-HPMTF	23.7	390.7	604.0
CS2-HPMTF-CLD	2.6	367.3	591.2
CS2-HPMTF-FL	8.9	392.6	605.6
CS2-HPMTF-FP	26.5	389.6	601.5
FG [⊗] (similar to CS2-HPMTF)	18	365	582
NV Base 1 [⊕] (similar to CS2-HPMTF)	18.8	189.0	526.7
NV Test 3 [⊕] (similar to CS2-HPMTF-CLD)	0.7	180.2	550.7
KH NEW_CHEM1 [⊗] (similar to CS2-HPMTF, with photolysis of HPMTF)	15.1	-	-
KH NEW_CHEM2 [⊗] (similar to CS2-HPMTF-FL)	6.1	-	-

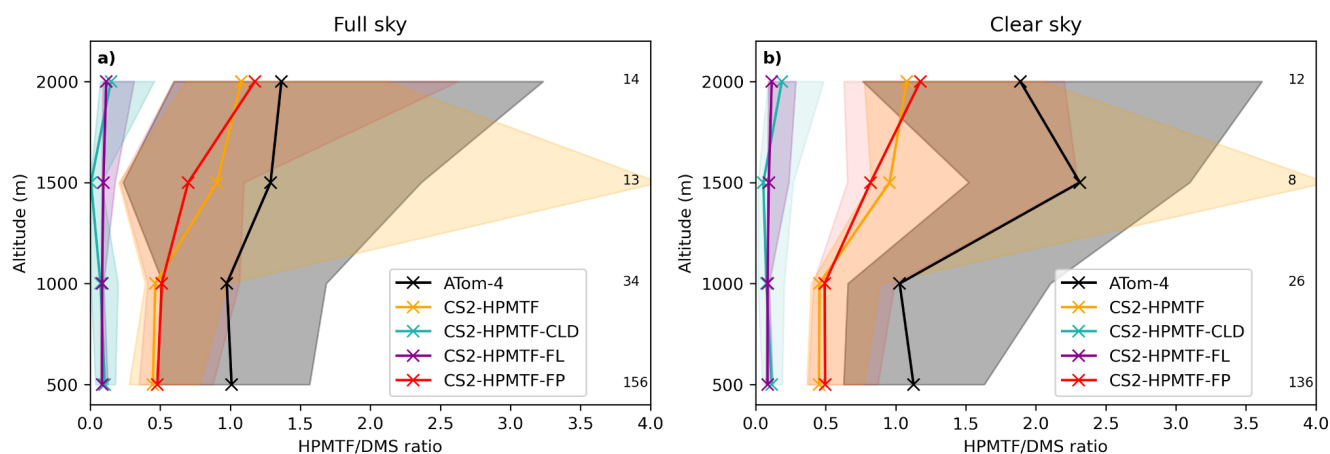
81 **4.3.1 HPMTF**

82 The HPMTF burden varies between 2.6 and 26.5 Gg S among the sensitivity runs (**Table 4**). Compared to CS2-HPMTF, faster
 83 OH oxidation reduces the HPMTF burden by -62% to 8.9 Gg S, while the addition of cloud and aqueous uptake to the scheme
 84 reduces it by -91% to only 2.6 Gg S. Yet, a factor of 5 higher production rate constant of HPMTF only leads to a 12% increase
 85 of HPMTF burden to 26.5 Gg S; suggesting that the steady-state distribution of HPMTF is controlled by the loss rate, not the
 86 rate of production of HPMTF. With the isomerization rate constant recommended by Veres et al. (2020), 51% of DMS forms
 87 HPMTF (86% of MTMP); with the faster rate in CS2-HPMTF-FP it is 57% (96% of MTMP). Since the use of the isomerization
 88 rate from Veres et al. (2020) already outcompetes the bimolecular reactions of MTMP, scaling the A-factor does not have a
 89 significant effect on the HPMTF yield from DMS. Overall, it can be estimated that globally 50-60% of DMS forms HPMTF
 90 (however, if more DMS is oxidised through the addition channel by BrO or multiphase reactions, this ratio could be lower).
 91 Consequently, HPMTF formation seems to be well constrained and the major uncertainties lie with the loss of HPMTF, which
 92 warrant additional measurements.

93

94 Similar to **Figure 10**, the HPMTF:DMS ratio is used in **Figure 13** to compare the results of the sensitivity model runs with
 95 ATom-4 observations. In general, schemes with a higher production and slower loss of HPMTF match the observations better,
 96 however, they still underestimate the measured ratios. A comparison was made to HPMTF:DMS ratios measured with no
 97 clouds present. Under these clear-sky conditions, when cloud uptake of HPMTF should not play a role in the measurements,
 98 observed ratios were even higher, leading to a greater difference between model results (which include clouds) and
 99 observations.

00



01

02 **Figure 13:** Vertically binned (500 m) median HPMTF/DMS ratio along the ATom-4 flight path for **a)** full sky and **b)** clear
03 sky, where measurements made in clouds are omitted. The envelopes represent the interquartile range of the measurements
04 and the respective model results, while values on the side give the number of measurements in the respective bin. Note that
05 the model data is the same in both panels.

06

07 **4.3.2 SO₂**

08 The SO₂ burden varies between 367.3 Gg S in CS2-HPMTF-CLD and 392.6 GgS in CS2-HPMTF-FL, suggesting that the SO₂
09 burden is relatively unaffected by the chemical sensitivities explored when compared with the much larger SO₂ burden simulated
10 with ST (469.7 Gg S); mainly due to the 100% DMS-SO₂ yield (**Table 4**).

11

12 CS2-HPMTF, CS2-HPMTF-FL, and CS2-HPMTF-FP have a higher SO₂ burden than CS2 since the changes to the abstraction
13 pathway (reaction 6a, 7c) and the addition of the isomerization pathway lead to more direct SO₂ production. Faster OH
14 oxidation of HPMTF in CS2-HPMTF-FL reduces the amount of HPMTF deposited and therefore increases the SO₂ burden
15 slightly (by 0.5%) compared to CS2-HPMTF. The faster production of HPMTF in CS2-HPMTF-FP reduces SO₂ burden
16 marginally (-0.3%), due to more sulfur now being deposited as HPMTF or forming OCS. The addition of cloud and
17 heterogeneous loss in CS2-HPMTF-CLD leads to immediate sulfate production instead of SO₂ formation, reducing the SO₂
18 burden by -6% compared to CS2-HPMTF, resulting in the lowest SO₂ burden in all runs considered.

19

20 **4.4.3 Sulfate**

21 In the sensitivity runs, the sulfate burdens are all higher than in the CS2 run (582.3 Gg S) and lower than in the ST run (635.9
22 Gg S). The variation by approximately 15 Gg S, from 591.2 Gg S in CS2-HPMTF-CLD to 605.6 Gg S in CS2-HPMTF-FL, is
23 smaller than the variation in sulfate burden simulated by similar mechanistic sensitivity tests by Novak et al. (2021) (~24 Gg),
24 suggesting some structural dependence on the results of the sensitivity tests (e.g., resolution, other model parameters). The
25 sulfate burdens in CS2-HPMTF-FL and CS2-HPMTF-FP behave similarly to CS2-HPMTF. Since CS2-HPMTF-CLD added
26 direct sulfate formation, a higher sulfate burden was expected. However, this was not seen in the experiments. Inspection of
27 the sulfate aerosol distribution shows that CS2-HPMTF-CLD leads to an increase in the coarse mode sulfate and a concomitant
28 reduction in sulfate aerosol lifetime (through an increase in wet deposition).

29

30

31 **5 Discussion**

32 The results described above demonstrate the global scale changes in the distribution of DMS and its oxidation products, through
33 the incorporation of improved mechanistic updates into the UKCA model. Here we discuss our results in the context of the
34 existing literature.

35 **5.1 DMS**

36 The DMS burden of 63-66 Gg S in this work is in good agreement with recent modelling studies (50 Gg S in Fung et al. (2022),
37 74 Gg S in Chen et al. (2018)). However, as shown in the supplement, S2.1.1, the modelled DMS concentrations do not match
38 observational measurements. One explanation could be underestimation of DMS oxidation. Here, only oxidation by OH and
39 NO₃ is included. However, Fung et al. (2022), who include oxidation by BrO, O₃ and Cl (accounting in total for 20% of DMS
40 depletion), also found that their model over-predicted DMS mixing ratios compared to the ATom-4 measurements. Inadequate
41 representation of DMS concentrations in seawater and therefore emissions contribute to the largest uncertainties in the sulfur
42 budget (Tesdal et al., 2016; Bock et al., 2021) and could explain most of the difference. Additionally, physical differences
43 between model and observation, such as wind speed and temperature, and a poor space resolution of Whole Air Sampling
44 might also play a role. Crucially, more long-term observations of DMS in the atmosphere are needed to complement works
45 that have collated oceanic DMS observations (e.g., Lana et al., 2011).

46
47 Here, in all model runs 75% of DMS is oxidised by OH and 25% by NO₃. Other studies found global contributions of OH
48 between 50-70% and NO₃ 15-30% (Boucher et al., 2003; Berglen et al., 2004; Breider et al., 2010; Khan et al., 2016; Chen et
49 al., 2018; Fung et al., 2022). The lower contribution of OH oxidation to DMS removal is explained by the addition of other
50 pathways, such as oxidation by BrO, Cl and multiphase reactions. Consequently, the lifetime of 1.5 days for DMS in this work
51 is longer than some other studies including these reactions (e.g., 0.8 days in Fung et al. (2022) and 1.2 days in Chen et al.
52 (2018)). Nonetheless, it is well within the range of 0.9 to 5 days (with a mean of 2 days) of the models examined in Faloon
53 (2009).

54
55

56 **5.2 HPMTF**

57 In CS₂-HPMTF 51% of DMS forms HPMTF. With a faster formation of HPMTF, found in laboratory experiments, this yield
58 increases to 57% in our model. The yield could possibly be lower if other oxidation reactions of DMS are included that follow
59 the OH addition pathway (multiphase reactions, oxidation by BrO), which was omitted in this work. Veres et al. (2020), Novak
60 et al. (2021) and Fung et al. (2022) estimated that at least 30-46% of DMS was forming HPMTF, based on observationally
61 constrained modelling of *in situ* or laboratory data. Even though the rate of HPMTF formation is uncertain (Ye et al., 2021),

62 it does not significantly affect the HPMTF yield from DMS, since it already outcompetes most other reactions of MTMP. For
63 HPMTF formation, uncertainty seems to lie mainly at the branching ratio of the addition and the abstraction pathway of DMS.
64 Indeed, the uncertainty in the HPMTF burden stems from the uncertainty in the loss pathways and their respective contribution
65 to HPMTF loss. Our model results agree well with the HPMTF burdens obtained by other global modelling studies, both in
66 absolute values but also the relative changes we find in the sensitivity study (**Table 4**) (e.g., Fung et al. (2022)): In our
67 sensitivity study a faster oxidation of HPMTF to OH lead to a decrease of 62% of the HPMTF burden, in Khan et al. (2021) it
68 was 60%. In this work the addition of aqueous uptake of HPMTF reduced the burden by 91%, very similar to the reduction
69 simulated in Novak et al. (2021) (96%).
70

71 **5.3 MSA**

72 The tropospheric MSA burden is 40 Gg S in CS2-HPMTF with a lifetime of 6 days. This falls within the range of 13-40 Gg S
73 and a lifetime of 5-7 days found in previous model studies (Pham et al., 1995; Chin et al., 1996, 2000; Cosme et al., 2002;
74 Hezel et al., 2011). However, newer studies include more multiphase processes and usually tend to have shorter lifetimes and
75 lower MSA burdens. Both the scheme in Fung et al. (2022) and Chen et al. (2018), include the loss of MSA to aqueous OH
76 oxidation, resulting in lifetimes of 0.6 days and 2.2 days and a burden of 8 Gg S and 20 Gg S, respectively.

77 **5.4 SO₂ and Sulfate**

78 Comparing SO₂ and sulfate burdens with other modelling studies is more challenging, since those species can have other
79 sources apart from DMS. That said, our SO₂ obtained in the various runs based on the CS2 scheme are comparable to Fung et
80 al. (2022), while the ST burden is significantly higher. However, the SO₂ burden from Novak et al. (2021) is much lower. This
81 difference cannot be explained solely by differences in the DMS oxidation mechanism; more likely, the difference is in
82 anthropogenic SO₂ emissions.

83 The sulfate burden in all our runs fall within the range found in other recent modelling studies (Chen et al. 2018; Novak et al.,
84 2021; Fung et al., 2022). Considering the relative change due to the addition of the isomerization pathway, the increase in
85 sulfate burden from CS2 to CS2-HPMTF is only 3.7% in our study, Fung et al. (2022) found an increase of 8.8%, when they
86 added HPMTF chemistry. However, unlike their results, we find strong seasonality in the additional sulfate produced,
87 especially in the Southern Hemisphere. The addition of cloud uptake and direct sulfate formation in CS2-HPMTF-CLD
88 decreased the sulfate burden in our study by (-)2.2%, in Novak et al. (2021) this change in mechanism lead to an increase of
89 sulfate by 4.5%.
90

91 **5.5 Comparison with BOXMOX results.**

92 In Section 3 and Section 4 we have shown the results of BOXMOX and UKCA simulations using different DMS mechanistic
93 variants respectively. Whilst the same mechanistic variants have been assessed in both model setups, it is not possible to

94 directly compare the results of the two sets of experiments because of the large differences in the model setups used. However,
95 some qualitative comparisons can be made. For MSA, Section 3.1 (**Figure 2**) suggests that the MSA simulated with CS2-
96 HPMTF should be much lower than CS2; as is calculated in Section 4.2.2 (a 70% reduction). For SO₂, both the BOXMOX
97 and UKCA results agree in the ordering of simulations, ST, CS2 and CS2-HPMTF; with ST simulating significantly more SO₂
98 than the other mechanisms. However, whereas BOXMOX simulations suggest that H₂SO₄ is predicted to be higher in CS2 and
99 CS2-HPMTF than ST, the UKCA model runs suggest that ST has the greatest burden of sulfate; highlighting the complexity
00 of making inference on aerosols from gas phase precursors in box model studies.

01

02 **6 Conclusion**

03 DMS remains an important molecule in our understanding of the background aerosol budget and the uncertainty of aerosols
04 to climate change (Carslaw et al., 2013). In this study we have used a combination of box modelling experiments and global
05 3D model experiments to explore the sensitivities of the DMS oxidation mechanism in the UKCA model. This work has
06 delivered a new DMS oxidation mechanism for use within the CRI-Strat framework of UKCA (Archer-Nicholls et al., 2021;
07 Weber et al., 2021), which is a significant advancement and improvement over the mechanism used in CMIP6 studies
08 (Archibald et al., 2020). Our new DMS mechanism includes many of the recently discovered and proposed oxidation pathways
09 for DMS and through the series of experiments we have performed, we have been able to benchmark this scheme against other
10 recently reported schemes in the literature. Our results suggest that as a priority laboratory studies are performed that address
11 1) the uptake of HPMTF onto aerosol surfaces and the products of this reaction. 2) The kinetics and products of the following
12 reactions: CH₃SO₃ decomposition; CH₃S + O₂; CH₃SOO decomposition; CH₃SO + O₃.

13

14 However, whilst future work building on the ever expanding database of laboratory studies (e.g., Ye et al., 2021; Jernigan et
15 al., 2022) are required to refine the DMS oxidation mechanism further, with the current availability of observational data, it is
16 not possible to fully constrain these DMS oxidation mechanisms using ambient observations. Hence there is a priority for
17 more observational based studies that combine ship, ground-based and aircraft platforms optimally. Fung et al. (2021) have
18 shown that there are consequences for radiative forcing by updating the DMS mechanism in the CESM model, and follow up
19 work will investigate these changes with UKCA.

20

21 This study adds to the few other mechanism intercomparisons that exist in the literature, spanning back more than 25 years
22 (Capaldo and Pandis 1997; Karl et al., 2007). Similar to these other studies we find that MSA is particularly uncertain when it
23 comes to the results obtained using the range of mechanisms that we investigated. Further work should explicitly focus on
24 reducing uncertainty in the MSA budget in the atmosphere, especially given its potential importance in reconstructing paleo-
25 sea ice (Thomas et al., 2019).

26

27 In many ways, the recent advances in DMS oxidation chemistry are similar to isoprene chemistry, where over a decade ago
28 the discovery of uni-molecular isomerisation reactions resulted in a step-change in our understanding of isoprene. As with
29 isoprene, ever more complex and faithful descriptions of DMS chemistry will be delivered over the coming years. But the
30 biggest challenge (as for isoprene) will remain in reducing and accurately distilling down this complex chemistry for use in
31 global model studies, and in characterising the sources of DMS into the atmosphere (which for isoprene have only recently
32 been possibly directly e.g., Wells et al., 2020).

33

34 **Acknowledgements**

35 BAC thanks the Studienstiftung des Deutschen Volkes for financial support. We would like to thank NERC through the ACSIS
36 (NE/N018001/1) and CARES projects for funding (NE/W009412/1). We would like to thank the UK Met Office JWCRP and
37 Clean Air programmes and the National Centre for Atmospheric Science for funding the development of the UKCA model.
38 LER acknowledges support from the Deep South National Science Challenge (contract C01X1901). ATA thanks the
39 University of Canterbury Erskine Programme. This work used Monsoon2, a collaborative high-performance computing facility
40 funded by the Met Office and the Natural Environment Research Council. This work used JASMIN, the UK collaborative data
41 analysis facility.

42

43 **Competing interests**

44 The authors declare no competing interests.

45 **References**

- 46 Assaf, E., Finewax, Z., Marshall, P., Veres, P.R., Neuman, J.A. and Burkholder, J.B.: Measurement of the Intramolecular
47 Hydrogen-Shift Rate Coefficient for the CH₃SCH₂OO Radical between 314 and 433 K. *The Journal of Physical Chemistry*
48 *A*, 127(10), pp.2336-2350, 2023.
- 49 Andreae, M. O.: Ocean-atmosphere interactions in the global biogeochemical sulfur cycle, *Marine Chemistry*, 30, 1–29,
50 [https://doi.org/10.1016/0304-4203\(90\)90059-L](https://doi.org/10.1016/0304-4203(90)90059-L), 1990.
- 51 Archer-Nicholls, S., Abraham, N. L., Shin, Y. M., Weber, J., Russo, M. R., Lowe, D., Utembe, S. R., O'Connor, F. M.,
52 Kerridge, B., Latter, B., Siddans, R., Jenkin, M., Wild, O., and Archibald, A. T.: The Common Representative Intermediates
53 Mechanism Version 2 in the United Kingdom Chemistry and Aerosols Model, 13, e2020MS002420,
54 <https://doi.org/10.1029/2020MS002420>, 2021.
- 55 Archibald, A. T., Jenkin, M. E., and Shallcross, D. E.: An isoprene mechanism intercomparison, *Atmospheric Environment*,
56 44, 5356–5364, <https://doi.org/10.1016/j.atmosenv.2009.09.016>, 2010.
- 57 Archibald, A. T., O'Connor, F. M., Abraham, N. L., Archer-Nicholls, S., Chipperfield, M. P., Dalvi, M., Folberth, G. A.,
58 Dennison, F., Dhomse, S. S., Griffiths, P. T., Hardacre, C., Hewitt, A. J., Hill, R. S., Johnson, C. E., Keeble, J., Köhler, M. O.,
59 Morgenstern, O., Mulcahy, J. P., Ordóñez, C., Pope, R. J., Rumbold, S. T., Russo, M. R., Savage, N. H., Sellar, A., Stringer,
60 M., Turnock, S. T., Wild, O., and Zeng, G.: Description and evaluation of the UKCA stratosphere–troposphere chemistry
61 scheme (StratTrop vn 1.0) implemented in UKESM1, 13, 1223–1266, <https://doi.org/10.5194/gmd-13-1223-2020>, 2020.
- 62 Arsene, C., Barnes, I., and Becker, K. H.: FT-IR product study of the photo-oxidation of dimethyl sulfide: Temperature and
63 O₂ partial pressure dependence, *Phys. Chem. Chem. Phys.*, 1, 5463–5470, <https://doi.org/10.1039/A907211J>, 1999.
- 64 Atkinson, R., Baulch, D. L., Cox, R. A., Crowley, J. N., Hampson, R. F., Hynes, R. G., Jenkin, M. E., Rossi, M. J., and Troe,
65 J.: Evaluated kinetic and photochemical data for atmospheric chemistry: Volume I - gas phase reactions of O_x, HO_x, NO_x and
66 SO_x species, 4, 1461–1738, <https://doi.org/10.5194/acp-4-1461-2004>, 2004.
- 67 Barnes, I., Hjorth, J., and Mihalopoulos, N.: Dimethyl Sulfide and Dimethyl Sulfoxide and Their Oxidation in the Atmosphere,
68 *Chem. Rev.*, 106, 940–975, <https://doi.org/10.1021/cr020529+>, 2006.
- 69 Barone, S., A. Turnipseed, A., and R. Ravishankara, A.: Role of adducts in the atmospheric oxidation of dimethyl sulfide, 100,
70 39–54, <https://doi.org/10.1039/FD9950000039>, 1995.
- 71 Berglen, T. F., Berntsen, T. K., Isaksen, I. S. A., and Sundet, J. K.: A global model of the coupled sulfur/oxidant chemistry in
72 the troposphere: The sulfur cycle, 109, <https://doi.org/10.1029/2003JD003948>, 2004.

73 Berndt, T., Scholz, W., Mentler, B., Fischer, L., Hoffmann, E. H., Tilgner, A., Hyttinen, N., Prisle, N. L., Hansel, A., and
74 Herrmann, H.: Fast Peroxy Radical Isomerization and OH Recycling in the Reaction of OH Radicals with Dimethyl Sulfide,
75 *J. Phys. Chem. Lett.*, 10, 6478–6483, <https://doi.org/10.1021/acs.jpcclett.9b02567>, 2019.

76 Bhatti, Y., Revell, L., Schuddeboom, A., McDonald, A., Archibald, A., Williams, J., Venugopal, A., Hardacre, C., and
77 Behrens, E.: The sensitivity of Southern Ocean atmospheric dimethyl sulfide to modelled sources and emissions, *EGUsphere*
78 [preprint], <https://doi.org/10.5194/egusphere-2023-868>, 2023.

79 Bock, J., Michou, M., Nabat, P., Abe, M., Mulcahy, J. P., Olivié, D. J. L., Schwinger, J., Suntharalingam, P., Tjiputra, J., van
80 Hulten, M., Watanabe, M., Yool, A., and Séférian, R.: Evaluation of ocean dimethylsulfide concentration and emission in
81 CMIP6 models, 18, 3823–3860, <https://doi.org/10.5194/bg-18-3823-2021>, 2021.

82 Borissenko, D., Kukui, A., Laverdet, G., and Le Bras, G.: Experimental Study of SO₂ Formation in the Reactions of CH₃SO
83 Radical with NO₂ and O₃ in Relation with the Atmospheric Oxidation Mechanism of Dimethyl Sulfide, *J. Phys. Chem. A*,
84 107, 1155–1161, <https://doi.org/10.1021/jp021701g>, 2003.

85 Boucher, O., Moulin, C., Belviso, S., Aumont, O., Bopp, L., Cosme, E., von Kuhlmann, R., Lawrence, M. G., Pham, M.,
86 Reddy, M. S., Sciare, J., and Venkataraman, C.: DMS atmospheric concentrations and sulphate aerosol indirect radiative
87 forcing: a sensitivity study to the DMS source representation and oxidation, 3, 49–65, <https://doi.org/10.5194/acp-3-49-2003>,
88 2003.

89 Breider, T. J., Chipperfield, M. P., Richards, N. a. D., Carslaw, K. S., Mann, G. W., and Spracklen, D. V.: Impact of BrO on
90 dimethylsulfide in the remote marine boundary layer, 37, <https://doi.org/10.1029/2009GL040868>, 2010.

91 de Bruyn, W. J., Harvey, M., Cainey, J. M., and Saltzman, E. S.: DMS and SO₂ at Baring Head, New Zealand: Implications
92 for the Yield of SO₂ from DMS, *Journal of Atmospheric Chemistry*, 41, 189–209, <https://doi.org/10.1023/A:1014252106572>,
93 2002.

94 Butkovskaya, N. I. and Barnes, I.: Model Study of the Photooxidation of CH₃SO₂SCH₃ at Atmospheric Pressure: Thermal
95 Decomposition of the CH₃SO₂ Radical, in: *Global Atmospheric Change and its Impact on Regional Air Quality*, edited by:
96 Barnes, I., Springer Netherlands, Dordrecht, 147–152, https://doi.org/10.1007/978-94-010-0082-6_22, 2002.

97 Butkovskaya, N. I. and LeBras, G.: Mechanism of the NO₃ + DMS Reaction by Discharge Flow Mass Spectrometry, *J. Phys.*
98 *Chem.*, 98, 2582–2591, <https://doi.org/10.1021/j100061a014>, 1994.

99 Caldeira, K. and Duffy, P.B. The role of the Southern Ocean in uptake and storage of anthropogenic carbon dioxide. *Science*,
00 287(5453), pp.620-622. 2000.

01 Campolongo, F., Saltelli, A., Jensen, N. R., Wilson, J., and Hjorth, J.: The Role of Multiphase Chemistry in the Oxidation of
02 Dimethylsulphide (DMS). A Latitude Dependent Analysis, *Journal of Atmospheric Chemistry*, 32, 327–356,
03 <https://doi.org/10.1023/A:1006154618511>, 1999.

04 Cao, J., Wang, W.L., Gao, L.J. and Fu, F.: Mechanism and thermodynamic properties of CH_3SO_3 decomposition. *Acta*
05 *Physico-Chimica Sinica*, 29(6), 1161-1167, <https://doi.org/10.3866/PKU.WHXB201304021>, 2013.

06 Capaldo, K.P. and Pandis, S.N. Dimethylsulfide chemistry in the remote marine atmosphere: Evaluation and sensitivity
07 analysis of available mechanisms. *Journal of Geophysical Research: Atmospheres*, 102(D19), pp.23251-23267. 1997

08

09 Carslaw, K. S., Lee, L. A., Reddington, C. L., Pringle, K. J., Rap, A., Forster, P. M., Mann, G. W., Spracklen, D. V.,
10 Woodhouse, M. T., Regayre, L. A., and Pierce, J. R.: Large contribution of natural aerosols to uncertainty in indirect forcing,
11 503, 67–71, <https://doi.org/10.1038/nature12674>, 2013.

12 Charlson, R. J., Lovelock, J. E., Andreae, M. O., and Warren, S. G.: Oceanic phytoplankton, atmospheric sulphur, cloud albedo
13 and climate, 326, 655–661, <https://doi.org/10.1038/326655a0>, 1987.

14 Chen, H. and Finlayson-Pitts, B. J.: New Particle Formation from Methanesulfonic Acid and Amines/Ammonia as a Function
15 of Temperature, *Environ. Sci. Technol.*, 51, 243–252, <https://doi.org/10.1021/acs.est.6b04173>, 2017.

16 Chen, H., Ezell, M. J., Arquero, K. D., Varner, M. E., Dawson, M. L., Gerber, R. B., and Finlayson-Pitts, B. J.: New particle
17 formation and growth from methanesulfonic acid, trimethylamine and water, *Phys. Chem. Chem. Phys.*, 17, 13699–13709,
18 <https://doi.org/10.1039/C5CP00838G>, 2015.

19 Chen, J., Berndt, T., Møller, K. H., Lane, J. R., and Kjaergaard, H. G.: Atmospheric Fate of the CH_3SOO Radical from the
20 $\text{CH}_3\text{S} + \text{O}_2$ Equilibrium, *J. Phys. Chem. A*, 125, 8933–8941, <https://doi.org/10.1021/acs.jpca.1c06900>, 2021.

21 Chen, Q., Sherwen, T., Evans, M., and Alexander, B.: DMS oxidation and sulfur aerosol formation in the marine troposphere:
22 a focus on reactive halogen and multiphase chemistry, 18, 13617–13637, <https://doi.org/10.5194/acp-18-13617-2018>, 2018.

23 Chin, M., Jacob, D. J., Gardner, G. M., Foreman-Fowler, M. S., Spiro, P. A., and Savoie, D. L.: A global three-dimensional
24 model of tropospheric sulfate, 101, 18667–18690, <https://doi.org/10.1029/96JD01221>, 1996.

25 Chin, M., Savoie, D. L., Huebert, B. J., Bandy, A. R., Thornton, D. C., Bates, T. S., Quinn, P. K., Saltzman, E. S., and Bruyn,
26 W. J. D.: Atmospheric sulfur cycle simulated in the global model GOCART: Comparison with field observations and regional
27 budgets, 105, 24689–24712, <https://doi.org/10.1029/2000JD900385>, 2000.

28 Collins, W. J., Lamarque, J.-F., Schulz, M., Boucher, O., Eyring, V., Hegglin, M. I., Maycock, A., Myhre, G., Prather, M.,
29 Shindell, D., and Smith, S. J.: AerChemMIP: quantifying the effects of chemistry and aerosols in CMIP6, 10, 585–607,
30 <https://doi.org/10.5194/gmd-10-585-2017>, 2017.

31 Cosme, E., Genthon, C., Martinerie, P., Boucher, O., and Pham, M.: The sulfur cycle at high-southern latitudes in the LMD-
32 ZT General Circulation Model, 107, ACH 7-1-ACH 7-19, <https://doi.org/10.1029/2002JD002149>, 2002.

33 Dee, D. P., Uppala, S. M., Simmons, A. J., Berrisford, P., Poli, P., Kobayashi, S., Andrae, U., Balmaseda, M. A., Balsamo, G.,
34 Bauer, P., Bechtold, P., Beljaars, A. C. M., van de Berg, L., Bidlot, J., Bormann, N., Delsol, C., Dragani, R., Fuentes, M.,
35 Geer, A. J., Haimberger, L., Healy, S. B., Hersbach, H., Hólm, E. V., Isaksen, L., Kállberg, P., Köhler, M., Matricardi, M.,
36 McNally, A. P., Monge-Sanz, B. M., Morcrette, J.-J., Park, B.-K., Peubey, C., de Rosnay, P., Tavolato, C., Thépaut, J.-N., and
37 Vitart, F.: The ERA-Interim reanalysis: configuration and performance of the data assimilation system, 137, 553–597,
38 <https://doi.org/10.1002/qj.828>, 2011.

39 Faloon, I.: Sulfur processing in the marine atmospheric boundary layer: A review and critical assessment of modeling
40 uncertainties, *Atmospheric Environment*, 43, 2841–2854, <https://doi.org/10.1016/j.atmosenv.2009.02.043>, 2009.

41 Fung, K. M., Heald, C. L., Kroll, J. H., Wang, S., Jo, D. S., Gettelman, A., Lu, Z., Liu, X., Zaveri, R. A., Apel, E., Blake, D.
42 R., Jimenez, J.-L., Campuzano-Jost, P., Veres, P., Bates, T. S., Shilling, J. E., and Zawadowicz, M.: Exploring DMS oxidation
43 and implications for global aerosol radiative forcing, 1–58, <https://doi.org/10.5194/acp-2021-782>, 2021.

44 Galí, M., Levasseur, M., Devred, E., Simó, R., and Babin, M.: Sea-surface dimethylsulfide (DMS) concentration from satellite
45 data at global and regional scales, *Biogeosciences*, 15, 3497–3519, <https://doi.org/10.5194/bg-15-3497-2018>, 2018.

46 Glasow, R. von, Sander, R., Bott, A., and Crutzen, P. J.: Modeling halogen chemistry in the marine boundary layer 1. Cloud-
47 free MBL, 107, ACH 9-1-ACH 9-16, <https://doi.org/10.1029/2001JD000942>, 2002.

48 Griffiths, P. T., Murray, L. T., Zeng, G., Shin, Y. M., Abraham, N. L., Archibald, A. T., Deushi, M., Emmons, L. K., Galbally,
49 I. E., Hassler, B., Horowitz, L. W., Keeble, J., Liu, J., Moeini, O., Naik, V., O'Connor, F. M., Oshima, N., Tarasick, D., Tilmes,
50 S., Turnock, S. T., Wild, O., Young, P. J., and Zanis, P.: Tropospheric ozone in CMIP6 simulations, *Atmos. Chem. Phys.*, 21,
51 4187–4218, <https://doi.org/10.5194/acp-21-4187-2021>, 2021.

52 Guenther, A. B., Jiang, X., Heald, C. L., Sakulyanontvittaya, T., Duhl, T., Emmons, L. K., and Wang, X.: The Model of
53 Emissions of Gases and Aerosols from Nature version 2.1 (MEGAN2.1): an extended and updated framework for modeling
54 biogenic emissions, 5, 1471–1492, <https://doi.org/10.5194/gmd-5-1471-2012>, 2012.

55 Hezel, P. J., Alexander, B., Bitz, C. M., Steig, E. J., Holmes, C. D., Yang, X., and Sciare, J.: Modeled methanesulfonic acid
56 (MSA) deposition in Antarctica and its relationship to sea ice, 116, <https://doi.org/10.1029/2011JD016383>, 2011.

57 Ho, S., Peng, L., Anthes, R. A., Kuo, Y.-H., and Lin, H.-C.: Marine Boundary Layer Heights and Their Longitudinal, Diurnal,
58 and Interseasonal Variability in the Southeastern Pacific Using COSMIC, CALIOP, and Radiosonde Data, *J. Climate*, 28,
59 2856–2872, <https://doi.org/10.1175/JCLI-D-14-00238.1>, 2015.

60 Hoesly, R. M., Smith, S. J., Feng, L., Klimont, Z., Janssens-Maenhout, G., Pitkanen, T., Seibert, J. J., Vu, L., Andres, R. J.,
61 Bolt, R. M., Bond, T. C., Dawidowski, L., Kholod, N., Kurokawa, J., Li, M., Liu, L., Lu, Z., Moura, M. C. P., O'Rourke, P.
62 R., and Zhang, Q.: Historical (1750–2014) anthropogenic emissions of reactive gases and aerosols from the Community
63 Emissions Data System (CEDS), 11, 369–408, <https://doi.org/10.5194/gmd-11-369-2018>, 2018.

64 Hoffmann, E. H., Tilgner, A., Schrödner, R., Brüner, P., Wolke, R., and Herrmann, H.: An advanced modeling study on the
65 impacts and atmospheric implications of multiphase dimethyl sulfide chemistry, *PNAS*, 113, 11776–11781,
66 <https://doi.org/10.1073/pnas.1606320113>, 2016.

67 Hoffmann, E. H., Heinold, B., Kubin, A., Tegen, I., and Herrmann, H.: The Importance of the Representation of DMS
68 Oxidation in Global Chemistry-Climate Simulations, 48, e2021GL094068, <https://doi.org/10.1029/2021GL094068>, 2021.

69 Hulswar, S., Simó, R., Galí, M., Bell, T. G., Lana, A., Inamdar, S., Halloran, P. R., Manville, G., and Mahajan, A. S.: Third
70 revision of the global surface seawater dimethyl sulfide climatology (DMS-Rev3), *Earth Syst. Sci. Data*, 14, 2963–2987,
71 <https://doi.org/10.5194/essd-14-2963-2022>, 2022.

72 Jenkin, M. E., Young, J. C., and Rickard, A. R.: The MCM v3.3.1 degradation scheme for isoprene, 15, 11433–11459,
73 <https://doi.org/10.5194/acp-15-11433-2015>, 2015.

74 Jenkin, M. E., Khan, M. A. H., Shallcross, D. E., Bergström, R., Simpson, D., Murphy, K. L. C., and Rickard, A. R.: The CRI
75 v2.2 reduced degradation scheme for isoprene, *Atmospheric Environment*, 212, 172–182,
76 <https://doi.org/10.1016/j.atmosenv.2019.05.055>, 2019.

77 Jernigan, C.M., Fite, C.H., Vereecken, L., Berkelhammer, M.B., Rollins, A.W., Rickly, P.S., Novelli, A., Taraborrelli, D.,
78 Holmes, C.D. and Bertram, T.H. Efficient Production of Carbonyl Sulfide in the Low-NOx Oxidation of Dimethyl Sulfide.
79 *Geophysical Research Letters*, 49(3), p.e2021GL096838. 2022.

80 Karl, M., Gross, A., Leck, C., and Pirjola, L.: Intercomparison of dimethylsulfide oxidation mechanisms for the marine
81 boundary layer: Gaseous and particulate sulfur constituents, 112, <https://doi.org/10.1029/2006JD007914>, 2007.

82 Khan, M. A. H., Gillespie, S. M. P., Razis, B., Xiao, P., Davies-Coleman, M. T., Percival, C. J., Derwent, R. G., Dyke, J. M.,
83 Ghosh, M. V., Lee, E. P. F., and Shallcross, D. E.: A modelling study of the atmospheric chemistry of DMS using the global
84 model, STOCHEM-CRI, *Atmospheric Environment*, 127, 69–79, <https://doi.org/10.1016/j.atmosenv.2015.12.028>, 2016.

85 Khan, M. A. H., Bannan, T. J., Holland, R., Shallcross, D. E., Archibald, A. T., Matthews, E., Back, A., Allan, J., Coe, H.,
86 Artaxo, P., and Percival, C. J.: Impacts of Hydroperoxymethyl Thioformate on the Global Marine Sulfur Budget, *ACS Earth*
87 *Space Chem.*, 5, 2577–2586, <https://doi.org/10.1021/acsearthspacechem.1c00218>, 2021.

88 Knote, C., Tuccella, P., Curci, G., Emmons, L., Orlando, J. J., Madronich, S., Baró, R., Jiménez-Guerrero, P., Luecken, D.,
89 Hogrefe, C., Forkel, R., Werhahn, J., Hirtl, M., Pérez, J. L., San José, R., Giordano, L., Brunner, D., Yahya, K., and Zhang,
90 Y.: Influence of the choice of gas-phase mechanism on predictions of key gaseous pollutants during the AQMEII phase-2
91 intercomparison, *Atmospheric Environment*, 115, 553–568, <https://doi.org/10.1016/j.atmosenv.2014.11.066>, 2015.

92 Lee, C., Martin, R. V., van Donkelaar, A., Lee, H., Dickerson, R. R., Hains, J. C., Krotkov, N., Richter, A., Vinnikov, K., and
93 Schwab, J. J.: SO₂ emissions and lifetimes: Estimates from inverse modeling using in situ and global, space-based
94 (SCIAMACHY and OMI) observations, *J. Geophys. Res.-Atmos.*, 116, D06304, <https://doi.org/10.1029/2010JD014758>,
95 2011.

96 McKee, M. L.: Theoretical study of the CH₃SOO radical, *Chemical Physics Letters*, 211, 643–648,
97 [https://doi.org/10.1016/0009-2614\(93\)80157-K](https://doi.org/10.1016/0009-2614(93)80157-K), 1993.

98 Minikin, A., Legrand, M., Hall, J., Wagenbach, D., Kleefeld, C., Wolff, E., Pasteur, E. C., and Ducroz, F.: Sulfur-containing
99 species (sulfate and methanesulfonate) in coastal Antarctic aerosol and precipitation, 103, 10975–10990,
00 <https://doi.org/10.1029/98JD00249>, 1998.

01 Mulcahy, J.P., Jones, C., Sellar, A., Johnson, B., Boutle, I.A., Jones, A., Andrews, T., Rumbold, S.T., Mollard, J., Bellouin,
02 N. and Johnson, C.E. Improved aerosol processes and effective radiative forcing in HadGEM3 and UKESM1. *Journal of*
03 *Advances in Modeling Earth Systems*, 10(11), pp.2786-2805. 2018.

04 Mulcahy, J. P., Johnson, C., Jones, C. G., Povey, A. C., Scott, C. E., Sellar, A., Turnock, S. T., Woodhouse, M. T., Abraham,
05 N. L., Andrews, M. B., Bellouin, N., Browse, J., Carslaw, K. S., Dalvi, M., Folberth, G. A., Glover, M., Grosvenor, D. P.,
06 Hardacre, C., Hill, R., Johnson, B., Jones, A., Kipling, Z., Mann, G., Mollard, J., O'Connor, F. M., Palmiéri, J., Reddington,
07 C., Rumbold, S. T., Richardson, M., Schutgens, N. A. J., Stier, P., Stringer, M., Tang, Y., Walton, J., Woodward, S., and Yool,
08 A.: Description and evaluation of aerosol in UKESM1 and HadGEM3-GC3.1 CMIP6 historical simulations, 13, 6383–6423,
09 <https://doi.org/10.5194/gmd-13-6383-2020>, 2020.

10 Novak, G. A., Fite, C. H., Holmes, C. D., Veres, P. R., Neuman, J. A., Faloona, I., Thornton, J. A., Wolfe, G. M., Vermeuel,
11 M. P., Jernigan, C. M., Peischl, J., Ryerson, T. B., Thompson, C. R., Bourgeois, I., Warneke, C., Gkatzelis, G. I., Coggon, M.
12 M., Sekimoto, K., Bui, T. P., Dean-Day, J., Diskin, G. S., DiGangi, J. P., Nowak, J. B., Moore, R. H., Wiggins, E. B., Winstead,
13 E. L., Robinson, C., Thornhill, K. L., Sanchez, K. J., Hall, S. R., Ullmann, K., Dollner, M., Weinzierl, B., Blake, D. R., and
14 Bertram, T. H.: Rapid cloud removal of dimethyl sulfide oxidation products limits SO₂ and cloud condensation nuclei
15 production in the marine atmosphere, *PNAS*, 118, <https://doi.org/10.1073/pnas.2110472118>, 2021.

16 Pacifico, F., Harrison, S. P., Jones, C. D., Arneth, A., Sitch, S., Weedon, G. P., Barkley, M. P., Palmer, P. I., Serça, D.,
17 Potosnak, M., Fu, T.-M., Goldstein, A., Bai, J., and Schurgers, G.: Evaluation of a photosynthesis-based biogenic isoprene
18 emission scheme in JULES and simulation of isoprene emissions under present-day climate conditions, 11, 4371–4389,
19 <https://doi.org/10.5194/acp-11-4371-2011>, 2011.

20 Pham, M., Müller, J.-F., Brasseur, G. P., Granier, C., and Mégie, G.: A three-dimensional study of the tropospheric sulfur
21 cycle, 100, 26061–26092, <https://doi.org/10.1029/95JD02095>, 1995.

22 Ranjithkumar, A., Gordon, H., Williamson, C., Rollins, A., Pringle, K., Kupc, A., Abraham, N. L., Brock, C., and Carslaw,
23 K.: Constraints on global aerosol number concentration, SO₂ and condensation sink in UKESM1 using ATom measurements,
24 Atmos. Chem. Phys., 21, 4979–5014, <https://doi.org/10.5194/acp-21-4979-2021>, 2021.

25 Sander, R.: Compilation of Henry's law constants (version 4.0) for water as solvent, Atmos. Chem. Phys., 15, 4399–4981,
26 <https://doi.org/10.5194/acp-15-4399-2015>, 2015, corrigendum, 2021.

27 Sandu, A. and Sander, R.: Technical note: Simulating chemical systems in Fortran90 and Matlab with the Kinetic PreProcessor
28 KPP-2.1, 6, 187–195, <https://doi.org/10.5194/acp-6-187-2006>, 2006.

29 Sciare, J., Mihalopoulos, N., and Dentener, F. J.: Interannual variability of atmospheric dimethylsulfide in the southern Indian
30 Ocean, J. Geophys. Res., 105, 26369–26377, <https://doi.org/10.1029/2000JD900236>, 2000.

31 Sciare, J., Baboukas, E., and Mihalopoulos, N.: Short-Term Variability of Atmospheric DMS and Its Oxidation Products at
32 Amsterdam Island during Summer Time, Journal of Atmospheric Chemistry, 39, 281–302,
33 <https://doi.org/10.1023/A:1010631305307>, 2001.

34 Sellar, A. A., Jones, C. G., Mulcahy, J. P., Tang, Y., Yool, A., Wiltshire, A., O'Connor, F. M., Stringer, M., Hill, R., Palmieri,
35 J., Woodward, S., Mora, L. de, Kuhlbrodt, T., Rumbold, S. T., Kelley, D. I., Ellis, R., Johnson, C. E., Walton, J., Abraham, N.
36 L., Andrews, M. B., Andrews, T., Archibald, A. T., Berthou, S., Burke, E., Blockley, E., Carslaw, K., Dalvi, M., Edwards, J.,
37 Folberth, G. A., Gedney, N., Griffiths, P. T., Harper, A. B., Hendry, M. A., Hewitt, A. J., Johnson, B., Jones, A., Jones, C. D.,
38 Keeble, J., Liddicoat, S., Morgenstern, O., Parker, R. J., Predoi, V., Robertson, E., Siahann, A., Smith, R. S., Swaminathan,
39 R., Woodhouse, M. T., Zeng, G., and Zerroukat, M.: UKESM1: Description and Evaluation of the U.K. Earth System Model,
40 11, 4513–4558, <https://doi.org/10.1029/2019MS001739>, 2019.

41 Sellar, A. A., Walton, J., Jones, C. G., Wood, R., Abraham, N. L., Andrejczuk, M., Andrews, M. B., Andrews, T., Archibald,
42 A. T., de Mora, L., Dyson, H., Elkington, M., Ellis, R., Florek, P., Good, P., Gohar, L., Haddad, S., Hardiman, S. C., Hogan,
43 E., Iwi, A., Jones, C. D., Johnson, B., Kelley, D. I., Kettleborough, J., Knight, J. R., Köhler, M. O., Kuhlbrodt, T., Liddicoat,
44 S., Linova-Pavlova, I., Mizielinski, M. S., Morgenstern, O., Mulcahy, J., Neining, E., O'Connor, F. M., Petrie, R., Ridley,
45 J., Rioual, J.-C., Roberts, M., Robertson, E., Rumbold, S., Seddon, J., Shepherd, H., Shim, S., Stephens, A., Teixeira, J. C.,
46 Tang, Y., Williams, J., Wiltshire, A., and Griffiths, P. T.: Implementation of U.K. Earth System Models for CMIP6, 12,
47 e2019MS001946, <https://doi.org/10.1029/2019MS001946>, 2020.

48 Stevenson, D. S., Zhao, A., Naik, V., O'Connor, F. M., Tilmes, S., Zeng, G., Murray, L. T., Collins, W. J., Griffiths, P. T.,
49 Shim, S., Horowitz, L. W., Sentman, L. T., and Emmons, L.: Trends in global tropospheric hydroxyl radical and methane
50 lifetime since 1850 from AerChemMIP, *Atmos. Chem. Phys.*, 20, 12905–12920, <https://doi.org/10.5194/acp-20-12905-2020>,
51 2020.

52 Sutton, R.T., McCarthy, G.D., Robson, J., Sinha, B., Archibald, A.T. and Gray, L.J. Atlantic multidecadal variability and the
53 UK ACSIS program. *Bulletin of the American Meteorological Society*, 99(2), pp.415-425. 2018.

54 Telford, P. J., Abraham, N. L., Archibald, A. T., Braesicke, P., Dalvi, M., Morgenstern, O., O'Connor, F. M., Richards, N. a.
55 D., and Pyle, J. A.: Implementation of the Fast-JX Photolysis scheme (v6.4) into the UKCA component of the MetUM
56 chemistry-climate model (v7.3), 6, 161–177, <https://doi.org/10.5194/gmd-6-161-2013>, 2013.

57 Tesdal, J.-E., Christian, J. R., Monahan, A. H., Salzen, K. von, Tesdal, J.-E., Christian, J. R., Monahan, A. H., and Salzen, K.
58 von: Evaluation of diverse approaches for estimating sea-surface DMS concentration and air–sea exchange at global scale,
59 *Environ. Chem.*, 13, 390–412, <https://doi.org/10.1071/EN14255>, 2015.

60 Thomas, E.R., Allen, C.S., Etourneau, J., King, A.C., Severi, M., Winton, V.H.L., Mueller, J., Crosta, X. and Peck, V.L.
61 Antarctic sea ice proxies from marine and ice core archives suitable for reconstructing sea ice over the past 2000 years.
62 *Geosciences*, 9(12), 506. 2019.

63 Turnipseed, A. A., Barone, S. B., and Ravishankara, A. R.: Observation of methylthiyl radical addition to oxygen in the gas
64 phase, *J. Phys. Chem.*, 96, 7502–7505, <https://doi.org/10.1021/j100198a006>, 1992.

65 Urbanski, S. P., Stickel, R. E., and Wine, P. H.: Mechanistic and Kinetic Study of the Gas-Phase Reaction of Hydroxyl Radical
66 with Dimethyl Sulfoxide, *J. Phys. Chem. A*, 102, 10522–10529, <https://doi.org/10.1021/jp9833911>, 1998.

67 Veres, P. R., Neuman, J. A., Bertram, T. H., Assaf, E., Wolfe, G. M., Williamson, C. J., Weinzierl, B., Tilmes, S., Thompson,
68 C. R., Thames, A. B., Schroder, J. C., Saiz-Lopez, A., Rollins, A. W., Roberts, J. M., Price, D., Peischl, J., Nault, B. A., Møller,
69 K. H., Miller, D. O., Meinardi, S., Li, Q., Lamarque, J.-F., Kupc, A., Kjaergaard, H. G., Kinnison, D., Jimenez, J. L., Jernigan,
70 C. M., Hornbrook, R. S., Hills, A., Dollner, M., Day, D. A., Cuevas, C. A., Campuzano-Jost, P., Burkholder, J., Bui, T. P.,
71 Brune, W. H., Brown, S. S., Brock, C. A., Bourgeois, I., Blake, D. R., Apel, E. C., and Ryerson, T. B.: Global airborne sampling
72 reveals a previously unobserved dimethyl sulfide oxidation mechanism in the marine atmosphere, *Proc Natl Acad Sci USA*,
73 117, 4505–4510, <https://doi.org/10.1073/pnas.1919344117>, 2020.

74 Vermeuel, M. P., Novak, G. A., Jernigan, C. M., and Bertram, T. H.: Diel Profile of Hydroperoxymethyl Thioformate:
75 Evidence for Surface Deposition and Multiphase Chemistry, *Environ. Sci. Technol.*, 54, 12521–12529,
76 <https://doi.org/10.1021/acs.est.0c04323>, 2020.

77 von Glasow, R. and Crutzen, P. J.: Model study of multiphase DMS oxidation with a focus on halogens, *Atmos. Chem. Phys.*,
78 4, 589–608, <https://doi.org/10.5194/acp-4-589-2004>, 2004.

79 Walters, D., Baran, A. J., Boutle, I., Brooks, M., Earnshaw, P., Edwards, J., Furtado, K., Hill, P., Lock, A., Manners, J.,
80 Morcrette, C., Mulcahy, J., Sanchez, C., Smith, C., Stratton, R., Tennant, W., Tomassini, L., Van Weverberg, K., Vosper, S.,
81 Willett, M., Browse, J., Bushell, A., Carslaw, K., Dalvi, M., Essery, R., Gedney, N., Hardiman, S., Johnson, B., Johnson, C.,
82 Jones, A., Jones, C., Mann, G., Milton, S., Rumbold, H., Sellar, A., Ujiie, M., Whittall, M., Williams, K., and Zerroukat, M.:
83 The Met Office Unified Model Global Atmosphere 7.0/7.1 and JULES Global Land 7.0 configurations, 12, 1909–1963,
84 <https://doi.org/10.5194/gmd-12-1909-2019>, 2019.

85 Wang, X., Jacob, D. J., Downs, W., Zhai, S., Zhu, L., Shah, V., Holmes, C. D., Sherwen, T., Alexander, B., Evans, M. J.,
86 Eastham, S. D., Neuman, J. A., Veres, P. R., Koenig, T. K., Volkamer, R., Huey, L. G., Bannan, T. J., Percival, C. J., Lee, B.
87 H., and Thornton, J. A.: Global tropospheric halogen (Cl, Br, I) chemistry and its impact on oxidants, 21, 13973–13996,
88 <https://doi.org/10.5194/acp-21-13973-2021>, 2021.

89 Weber, J., Archer-Nicholls, S., Griffiths, P., Berndt, T., Jenkin, M., Gordon, H., Knote, C., and Archibald, A. T.: CRI-HOM:
90 A novel chemical mechanism for simulating highly oxygenated organic molecules (HOMs) in global chemistry–aerosol–
91 climate models, *Atmos. Chem. Phys.*, 20, 10889–10910, <https://doi.org/10.5194/acp-20-10889-2020>, 2020.

92 Weber, J., Archer-Nicholls, S., Abraham, N. L., Shin, Y. M., Bannan, T. J., Percival, C. J., Bacak, A., Artaxo, P., Jenkin, M.,
93 Khan, M. A. H., Shallcross, D. E., Schwantes, R. H., Williams, J., and Archibald, A. T.: Improvements to the representation
94 of BVOC chemistry–climate interactions in UKCA (v11.5) with the CRI-Strat 2 mechanism: incorporation and evaluation, 14,
95 5239–5268, <https://doi.org/10.5194/gmd-14-5239-2021>, 2021.

96 Wells, K.C., Millet, D.B., Payne, V.H., Deventer, M.J., Bates, K.H., de Gouw, J.A., Graus, M., Warneke, C., Wisthaler, A.
97 and Fuentes, J.D. Satellite isoprene retrievals constrain emissions and atmospheric oxidation. *Nature*, 585(7824), 225-233.
98 2020.

99 Wennberg, P. O., Bates, K. H., Crouse, J. D., Dodson, L. G., McVay, R. C., Mertens, L. A., Nguyen, T. B., Praske, E.,
00 Schwantes, R. H., Smarte, M. D., St Clair, J. M., Teng, A. P., Zhang, X., and Seinfeld, J. H.: Gas-Phase reactions of isoprene
01 and its major oxidation products, *Chem. Rev.*, 118, 3337–3390, <https://doi.org/10.1021/acs.chemrev.7b00439>, 2018.

02 Wofsy, S. C., Afshar, S., Allen, H. M., Apel, E. C., Asher, E. C., Barletta, B., Bent, J., Bian, H., Biggs, B. C., Blake, D. R.,
03 Blake, N., Bourgeois, I., Brock, C. A., Brune, W. H., Budney, J. W., Bui, T. P., Butler, A., Campuzano-Jost, P., Chang, C. S.,
04 Chin, M., Commane, R., Corr, G., and Zeng, L. H.: ATom: merged atmospheric chemistry, trace gases, and aerosols, data set,
05 ORNL DAAC, Oak Ridge, Tennessee, USA, <https://doi.org/10.3334/ORNLDAAC/1581>, 2018.

06 Wollesen de Jonge, R., Elm, J., Rosati, B., Christiansen, S., Hyttinen, N., Lüdemann, D., Bilde, M., and Roldin, P.: Secondary
07 aerosol formation from dimethyl sulfide – improved mechanistic understanding based on smog chamber experiments and
08 modelling, 21, 9955–9976, <https://doi.org/10.5194/acp-21-9955-2021>, 2021.

09 Wu, R., Wang, S., and Wang, L.: New Mechanism for the Atmospheric Oxidation of Dimethyl Sulfide. The Importance of
10 Intramolecular Hydrogen Shift in a CH₃SCH₂OO Radical, *J. Phys. Chem. A*, 119, 112–117, <https://doi.org/10.1021/jp511616j>,
11 2015.

12 Ye, Q., Goss, M. B., Isaacman-VanWertz, G., Zaytsev, A., Massoli, P., Lim, C., Croteau, P., Canagaratna, M., Knopf, D. A.,
13 Keutsch, F. N., Heald, C. L., and Kroll, J. H.: Organic Sulfur Products and Peroxy Radical Isomerization in the OH Oxidation
14 of Dimethyl Sulfide, *ACS Earth Space Chem.*, <https://doi.org/10.1021/acsearthspacechem.1c00108>, 2021.

15